HHS Public Access

Author manuscript

Nature. Author manuscript; available in PMC 2021 July 16.

Published in final edited form as:

Nature. 2020 October ; 586(7830): 623–627. doi:10.1038/s41586-020-2645-6.

PCNA activates the MutLγ endonuclease to promote meiotic crossing over

Dhananjaya S. Kulkarni[#1], **Shannon N. Owens**[#1], **Masayoshi Honda**[1,‡], **Masaru Ito**[1,*f*], **Ye Yang**[2,§], **Mary W. Corrigan**[1], **Lan Chen**[1], **Aric L. Quan**[1], **Neil Hunter**[1,2,3,*]

[1]Howard Hughes Medical Institute, University of California, Davis, Davis, California, USA.

[2]Department of Microbiology & Molecular Genetics, University of California, Davis, Davis, California, USA.

[3]Department of Molecular & Cellular Biology, University of California, Davis, Davis, California, USA.

[#] These authors contributed equally to this work.

SUMMARY

During meiosis, crossover recombination connects homologous chromosomes to direct their accurate segregation[1]. Defective crossing over causes infertility, miscarriage and congenital disease. Accordingly, each pair of chromosomes attains at least one crossover through processes that designate and then implement crossing over with high efficiency. At the DNA level, crossing over is implemented through the formation and biased resolution of double-Holliday Junction (dHJ) intermediates[2,3]. A central tenet of crossover resolution is that the two Holliday junctions (HJs) are resolved in opposite planes by targeting nuclease incisions to specific DNA strands[4]. The endonuclease activity of the MutLγ complex has been implicated in crossover-biased resolution[5–10], but mechanisms that activate and direct strand-specific cleavage remain unknown. Here we show that the sliding clamp, PCNA, is important for crossover-biased resolution. *In vitro* assays with human enzymes reveal that hPCNA and its loader hRFC are sufficient to activate the hMutLγ endonuclease. In this context, hMutLγ is further stimulated by a co-dependent activity of pro-crossover factors hEXO1 and hMutSγ, the latter of which binds HJs[11]. hMutLγ also specifically binds a variety of branched DNAs, including HJs, but canonical resolvase activity is

[*]Correspondence to: Neil Hunter, Department of Microbiology & Molecular Genetics, University of California, Davis, Davis, California, USA. nhunter@ucdavis.edu.

[‡]Current address: Carver College of Medicine, University of Iowa, Iowa City, Iowa, USA.

[*f*]Current address: Institute for Protein Research, Osaka University, Osaka, Japan

[§]Current address: ScienCell Research Laboratories, Carlsbad, California, USA.

Author Contributions

D.S.K., S.N.O., M.H. and N.H. conceived the study and designed most experiments. D.S.K. and M.H. performed all enzyme purifications and assays. S.N.O. performed all yeast experiments. M.I. performed the mouse cytology. All other authors assisted with experiments and data analysis. D.S.K., S.N.O. and N.H. wrote the manuscript with inputs and edits from all authors.

Competing interests

The authors declare no competing interests.

Data and Materials Availability Statement

Relevant data generated or analyzed during this study are included in this article and its supplementary information file. Biological materials are available from the corresponding author.

not observed implying that the endonuclease incises adjacent to junction branch points to effect resolution. *In vivo*, we show that budding yeast RFC facilitates MutLγ-dependent crossing over. Furthermore, PCNA localizes to prospective crossover sites along synapsed chromosomes. These data highlight similarities between crossover-resolution and the initiation steps of DNA mismatch repair[12,13] and evoke a novel model for crossover-specific dHJ resolution during meiosis.

Meiotic recombination initiates with DNA double-strand breaks (DSBs) and proceeds via homologous pairing and strand-exchange to form joint-molecule (JM) intermediates[1]. Regulatory processes designate a subset of events to become crossovers, and at these sites nascent JMs mature into dHJs. Through poorly defined mechanisms, MutLγ (comprising MLH1 and MLH3) accumulates at prospective crossover sites and biases dHJ resolution to specifically produce crossovers[1,14]. When MutLγ is dysfunctional, dHJs are still resolved, but with a non-crossover outcome[6]. Consequently, chromosome segregation fails and fertility is diminished. MLH1 and MLH3 are conserved members of the MutL family of DNA mismatch-repair (MMR) factors that couple mismatch-recognition by a MutS complex to downstream excision and resynthesis of the nascent strand[15]. MutL complexes from diverse species possess endonuclease activity that provides an initiation site for mismatch excision by a 5'−3' exonuclease such as EXO1[12,13]. During DNA replication, MutL-catalyzed incision, and thus MMR, is specifically targeted to the nascent strand via an orientation-specific interaction with the replicative clamp – PCNA in eukaryotes or the β-clamp in prokaryotes[16–19]. Endonuclease activity has been demonstrated for budding yeast and human MutLγ[8–10,20,21] and the conserved metal-binding active site in MLH3 is required for crossing over in both yeast[5,6] and mouse[7]. How the MutLγ endonuclease is activated and directed to effect crossover-specific dHJ resolution remains unknown.

Endonuclease activity of human MutLγ

Human MutLγ (hMutLγ) was purified from insect cells and endonuclease activity monitored using a supercoiled-plasmid DNA nicking assay (Fig. 1a and Extended Data Fig. 1). In isolation, hMutLγ displayed concentration-dependent nicking activity that required Mn^{2+} and the metal-binding site of hMLH3 indicating that activity was specific to hMutLγ (Extended Data Fig. 1). Endonuclease activity was not seen with Mg^{2+}, which is inferred to be the physiological metal cofactor[15,16]. Although Zn^{2+} is present at MutL active sites[15], nicking was also negligible with Zn^{2+} as well as Ca^{2+}, Ni^{2+}, Co^{2+} or Cd^{2+} (Extended Data Fig. 2). However, these metals competed with Mn^{2+} to inhibit hMutLγ endonuclease activity suggesting that Mn^{2+} is relatively weakly bound, and likely to be non-physiological[15]. The strict dependence on Mn^{2+} is analogous to human and yeast MutLα complexes (MLH1-PMS2 and Mlh1-Pms1, respectively) when assayed in isolation[16,22], but contrasts yeast MutLγ, which was reported to show endonuclease activity with a range of metals[9].

MutL proteins are ATPases; binding and hydrolysis of ATP is required for mismatch correction and meiotic crossover functions of yeast MutLγ *in vivo*[23], and induces conformational changes *in vitro*[20]. Typically, ATP stimulates MutL endonuclease activity[15], but surprisingly stimulation was not seen for budding yeast MutLγ, raising the possibility

that MutLγ complexes are distinctly regulated[8,9]. On the contrary, we observed that the human MutLγ endonuclease was stimulated 2-fold by ATP, when both Mn^{2+} and Mg^{2+} were present (Fig. 1b and Extended Data Fig. 2). Non-hydrolyzable ATP analogs, ATP-γ-S (adenosine 5′-[γ-thio]-triphosphate) and AMP-PNP (adenylyl-imidodiphosphate), did not stimulate hMutLγ endonuclease suggesting that ATP hydrolysis is required.

hMutSγ stimulates hMutLγ endonuclease

The MutSγ complex, MSH4-MSH5, specifically binds JM structures[11,24] (Extended Data Fig. 3c,d) and plays an earlier and more general role than MutLγ, localizing to a majority of meiotic recombination sites where it stabilizes nascent JMs to facilitate chromosome synapsis and dHJ formation[1,14,24,25]. The MMR paradigm predicts that MutSγ may also guide and trigger the MutLγ endonuclease[12,13]. However, MutLγ has its own JM binding activity[8,20](below), appears on synapsed chromosomes much later than MutSγ and localizes only to crossover sites[1,14], raising the possibility that MutLγ acts autonomously during dHJ resolution. Moreover, previous analysis of the yeast enzymes did not detect stimulation of the MutLγ endonuclease by MutSγ[8].

By co-immunostaining mouse spermatocyte chromosome spreads for MLH1 and MSH4, we revealed that as MutLγ first appears at prospective crossover sites in the mid-pachytene stage, it closely colocalizes with a subset of MutSγ foci (Fig. 1c,d and Extended Data Fig. 4). Co-localization was transient as MSH4 foci subsequently disappeared in late pachytene, while MutLγ persisted. This observation suggests mammalian MutSγ and MutLγ may transiently interact to modulate MutLγ endonuclease activity. To test this possibility, human MutSγ was purified and added to hMutLγ nicking assays (Fig. 1e,f and Extended Data Fig. 3a,f,g). Time-course analysis revealed >1.5-fold stimulation of MutLγ endonuclease activity by MutSγ that was ATP dependent. Notably, MutSγ provoked formation of a linearized plasmid product that arose with approximately the same timing as nicked product suggesting localized concerted incision of both DNA strands by MutLγ.

A nuclease-independent activity of EXO1 facilitates crossing over along the MutLγ pathway[26,27]. We also examined whether nuclease-dead hEXO1-D173A could enhance hMutLγ endonuclease, with or without hMutSγ, but additional stimulation was not seen under these conditions (Mn^{2+}, Mg^{2+} and ATP; Extended Data Fig. 3e–g, but see below and Figs. 2 and 3).

RFC-PCNA activates hMutLγ

Although Mn^{2+} activates MutL endonucleases, its physiological relevance is questionable[15]. In reconstituted mismatch-repair reactions with Mg^{2+} as the sole metal cofactor, MutL complexes are latent endonucleases, triggered only in the presence of heteroduplex DNA, a cognate MutS complex and loaded replicative clamp[15,16,18]. When the human clamp, hPCNA, and its loader, hRFC, were added to hMutLγ endonuclease reactions containing Mn^{2+} and ATP, nicking was enhanced more than two-fold, but only for an ensemble including both hMutSγ and hEXO1-D173A, implying concerted action of all five proteins (Fig. 2a and Extended Data Fig. 5). Strikingly, hRFC-hPCNA strongly activated the latent

hMutLγ endonuclease when Mg^{2+} was the sole metal cofactor (Fig. 2b and Extended Data Fig. 5). While hRFC-hPCNA alone could trigger hMutLγ, nicking was further stimulated >1.5-fold when both hMutSγ and hEXO1-D173A were also present, i.e. under these conditions hMutSγ and hEXO1-D173A appear to act as a largely interdependent stimulatory factor. In Mg^{2+}-only reactions, nicking was absolutely dependent on both hRFC (Fig. 2b, lane 9) and ATP (Extended Data Fig. 5), implying that hPCNA must be loaded onto DNA to activate hMutLγ. Moreover, hPCNA and hMutLγ interacted in solution, suggesting activation via direct association (Extended Data Fig. 5). Importantly, in these ensemble reactions, all nuclease activity required the metal-binding site of hMLH3, ruling out contaminating nucleases (Extended Data Fig. 5).

hMutLγ binds and is stimulated by HJs

Both budding yeast and human MutLγ preferentially bind branched DNA structures, including HJs [8,20], although Ranjha et al. reported binding was highly sensitive to salt and Mg^{2+} [8]. In our hands, hMutLγ selectively bound a variety of branched DNA substrates in the presence of physiological concentrations of salt and Mg^{2+} and excess competitor DNA (poly(dI-dC)) (Fig. 3a,b). Four-armed structures bound by hMutLγ included the pro-HJ (pHJ) containing one single-stranded (ss) arm, which approximates an initial D-loop[11]; a HJ with a 20 nt single-stranded gap in one arm (gHJ), a HJ with a nick at the junction point (nHJ); and a standard HJ (HJ; Fig. 3a). HJs and nHJs were bound with similar affinities (apparent K_d ~38 and ~39 nM, respectively; Fig. 3b) indicating that additional flexibility around the junction point does not influence hMutLγ binding (unlike, for example, the structure-selective endonuclease Mus81-$Mms4^{EME1}$ [28]). hMutLγ had significantly higher affinities for pHJ and gHJ substrates (apparent K_d ~14 and 16 nM, respectively) suggesting ssDNA enhances binding (Fig. 3b). Indeed, analogous to the budding yeast enzyme[20], hMutLγ was able to interact with ssDNA independently of its junction binding activity (Extended Data Fig. 6).

Despite the JM binding ability of hMutLγ, resolution or even nicking of model HJ substrates was not detected (Extended Data Fig. 7) implying that hMutLγ cannot catalyze symmetric incisions across the junction, i.e. it is not a classical HJ resolving enzyme. However, the presence of a HJ did influence binding and incision of a plasmid substrate (Fig. 3c–e and Extended Data Fig. 8). pUC(AT) contains an $(AT)_{20}$ inverted repeat that extrudes into a four-way hairpin junction upon supercoiling, but is otherwise identical to pUC19. By agarose-gel electrophoresis, a heterogeneous smear of hMutLγ–pUC19 complexes was observed suggesting unstable binding (Fig. 3c). By contrast, hMutLγ–pUC(AT) complexes migrated as relatively discrete species and overall efficiency of stable complex formation was much higher (Fig. 3d). Moreover, the decreasing mobility of hMutLγ–pUC(AT) complexes observed with increasing hMutLγ concentration points to formation of higher-order complexes analogous to the cooperative, multimeric oligomers described for yeast MutLγ[10,20].

In ensemble plasmid-nicking reactions with Mg^{2+} and ATP, pUC(AT) was incised up to 28% more efficiently than pUC19 (Fig. 3e, compare lanes 5 and 12; and lanes 7 and 14; also see Extended Data Fig. 8). Analogous to pUC19, pUC(AT) cleavage was most efficient when

hMutLγ, hMutSγ, hEXO1-D173A and hRFC-hPCNA were present, with hMutSγ and EXO1-D173A appearing to function interdependently (Extended Data Fig. 8). Distinct from pUC19, however, pUC(AT) incision was not absolutely dependent on hRFC-hPCNA, with 17% nicked product being formed in reactions containing hMutLγ, hMutSγ and hEXO1-D173A (Fig. 3e, compare lanes 4 and 11). Thus, the HJ in pUC(AT) modulates both the binding and incision of DNA by hMutLγ.

RFC-PCNA facilitates crossing over

A role for RFC-PCNA in MutLγ−dependent crossing over was demonstrated *in vivo* in budding yeast. An auxin-inducible degron (AID) allele of Rfc1 was used to inactivate RFC, and thereby prevent PCNA loading, precisely at the time of dHJ resolution (Fig. 4a; Rfc1-AID was employed because AID alleles of PCNA were not functional). An inducible allele of *NDT80* allowed reversible arrest of cells at the pachytene stage of meiosis, in which chromosomes are fully-synapsed and dHJs are poised for resolution[2]. Following addition of auxin and release from arrest, Rfc1-AID was rapidly degraded (Fig. 4b,c) and crossing over at a recombination hotspot was reduced from 17.5% (± 2.2% SEM) to 10.4% (± 1.8% SEM) (Fig. 4d,e). Similar analysis of *RFC1-AID mlh3Δ* cells indicated that RFC promotes primarily MutLγ−dependent crossovers. However, approximately one-third of *MLH3*-independent crossovers also appeared to be RFC dependent. This may be explained by the ability of RFC-PCNA to also stimulate structure-selective endonuclease, Mus81-Mms4^{EME1} [29], which defines a second crossover pathway in budding yeast[6]. Rfc1-AID degradation did not alter the timing or efficiency of dHJ resolution indicating that the crossover outcome, but not resolution *per se*, is promoted by RFC-PCNA (Fig. 4f, and Extended Data Fig. 9). Under these conditions, *mlh3Δ* mutation slightly delayed dHJ turnover, but resolution was ultimately efficient and Rfc1-AID degradation did not further alter the timing or efficiency of resolution.

Consistent with a role for RFC-PCNA in crossing over, PCNA localized to a subset of prospective crossover sites marked by the Zip3 protein (Fig. 4g)[30]. In chromosome spreads from cells arrested in pachytene, PCNA and Zip3 immunostaining foci averaged 15.4 (± 1.1 SEM) and 47.2 (± 1.3 SEM), respectively (n=25 nuclei); and 85.4% (± 1.9% SEM) of PCNA foci colocalized with Zip3 (random co-localization was estimated at 30.2% ± 2.4 SEM).

Discussion

Asymmetric incision is required for crossover-biased resolution of dHJs during meiosis, but how asymmetry is imposed has remained unclear. The requirements for MutSγ, MutLγ and EXO1 in meiotic crossing over evoke a MMR-like mechanism, involving MutLγ-catalyzed nicking of dHJs[1,14,25]. Our discoveries implicating RFC-PCNA in MutLγ-dependent crossing over strongly suggest that dHJ resolution is indeed similar to the initiation steps of MMR. We propose a specific model for crossover-specific dHJ resolution in which orientation-specific loading of PCNA, during the DNA synthesis that accompanies dHJ formation, helps direct the MutLγ-MutSγ-EXO1 ensemble to incise specific DNA strands on both sides of the junction points (Fig. 4h). In reconstituted MMR reactions, PCNA loaded

at a nick signals over hundreds of base pairs to direct incision of the same non-continuous strand by MutLα[12,13,15]. While incisions are biased upstream of the mismatch, in order to initiate excision by the 5'−3' exonuclease EXO1, nicking also occurs at downstream locations. By analogy, we propose that PCNA molecules loaded during recombination-associated DNA synthesis direct strand-specific nicking by MutLγ on both sides of the two HJs (Fig. 4h and Extended Data Fig. 10). Resolution occurs only when HJs adopt one of two co-axially stacked-X conformers, which could be favored by binding of MutSγ[24] or other pro-crossover factors. Critically, this model of dHJ resolution always specifies a crossover outcome. We suggest that the near continuous duplexes formed by stacked HJ arms enable the strand-specificity of PCNA-directed MutLγ-catalyzed incisions to be maintained across the junction points, even though the targeted strands are not actually contiguous. Given that nicking occurs some distance from the HJs, our model predicts that migration via a helicase will be required for resolution, consistent with the known role of RecQ-family helicase Sgs1/BLM[1,6]. Our model provides a solution to the critical question of how a crossover outcome is enforced at designated sites to help ensure accurate chromosome segregation during meiosis.

METHODS

Purification hMutLγ

MBP-hMLH3-His [8] and untagged hMLH1 [16] were co-expressed in insect cells according to standard protocols (Bac-to-Bac system, Invitrogen) and hMutLγ was purified as described by Ranjha et al.[8] with the following modifications. *Spodoptera frugiperda* Sf9 cells were coinfected with optimized ratios of baculoviruses, cells were harvested 52 h after infection, washed with phosphate-buffered saline (PBS), frozen in liquid nitrogen and stored at −80°C. A typical purification was performed with cell pellets from 3.6 L of culture. All subsequent steps were carried out at <4°C. Cells were resuspended in 3 volumes of lysis buffer (50 mM HEPES-NaOH pH 7.4, 1 mM DTT, 1 mM EDTA, 1:500 (v/v) protease inhibitor cocktail (P8340 Sigma), 1 mM phenylmethylsulfonyl fluoride, 30 μg/ml leupeptin) and stirred slowly for 15 min. Glycerol was added to 16% and 5 M NaCl was added for an final concentration of 325 mM. The sample was stirred for 30 min and then centrifuged at 50,000 g for 30 min. The clarified extract was bound in batch mode to 8 ml of pre-equilibrated amylose resin (New England Biolabs) for 1 hr. The resin was then washed extensively with 300 ml of buffer a buffer comprising 50 mM HEPES-NaOH pH 7.4, 2 mM β-mercaptoethanol, 250 mM NaCl, 10 % glycerol, 1 mM phenylmethylsulfonyl fluoride, 10 μg/ml leupeptin. Bound protein was eluted in wash buffer containing 10 mM maltose. Next, the MBP tag was cleaved from MLH3 with PreScission protease at a 1:16 ratio of proteins for 1 hr. The sample was applied to a pre-equilibrated 1 ml nickel-nitrilotriacetic acid resin column (Ni-NTA, Qiagen) over a 45 min period in wash buffer supplemented with 20 mM imidazole. The column was then washed under gravity flow with 100 ml buffer containing 60 mM imidazole, before eluting bound protein with the same wash buffer containing 400 mM imidazole. Pooled fractions were dialyzed against a buffer containing 25 mM HEPES-NaOH pH 7.4, 1 mM DTT 150 mM NaCl, 20% glycerol, 0.5 mM phenylmethylsulfonyl, concentrated with 50 kDa cut-off Amicon centrifugal filters (Millipore), and stored at 4 or 80 °C. Nuclease deficient hMutLγ (containing hMLH3-D1223N) was created by using a

QuikChange II Site-Directed Mutagenesis Kit (Agilent Technologies Inc, 200524). hMutLγ containing hMLH3-D1223N protein was prepared in the same way as wild-type protein. Protein concentrations were determined by Bradford assay using Bovine serum albumin as a standard, and by spectroscopic absorption at 280 nm.

Purification of hMutSγ

hMSH4 and *hMSH5–6His* coding regions were synthesized (GeneCopoeia), digested with SmaI and KpnI (for *MSH4*) or SalI and XbaI (for *MSH5–6His*) and cloned into the pFastBac Dual vector (ThermoFisher). Baculoviruses were prepared according to manufacturer's instructions and hMutSγ was purified as described previously[11] Insect cells were infected with hMSH4/hMSH5–6His baculovirus at 1×10^6 per mL, and incubated at 27°C for 56 hrs with shaking. Cells were centrifuged at 2000 rpm for 10 minutes at 4°C, washed with ice cold PBS, frozen in liquid nitrogen and stored at −80°C. A typical purification was performed with cell pellets from 1.6 L of culture. All subsequent steps were carried out at <4°C. Cells were thawed on ice-cold water for 5 min and then resuspended in 4 volumes of lysis buffer (25 mM HEPES pH 8.1, 300 mM NaCl, 20 mM imidazole, 10% glycerol, 500 uM PMSF, 10 μg/mL Pepstatin (Sigma), 10 μg/mL Leupeptin (Sigma), 10 μg/mL Aprotinin (Sigma), 1 μg/ml E-64 (Sigma) and lysate was passed five times through a 25G needle. The lysate was centrifuged at 35,000 rpm for 1 hour at 4°C, and clarified extract was loaded onto a 5 ml Ni-NTA column (GE Healthcare) pre-equilibrated with Buffer A (25 mM HEPES-NaOH pH 8.1, 300 mM NaCl, 20 mM Imidazole, 10% glycerol containing 500 μM PMSF, 1 μg/mL Pepstatin, and 1 μg/mL Leupeptin). The column was washed with 20 column volumes of Buffer A and then protein was eluted with a linear gradient of imidazole (20–300 mM) in Buffer A. Peak fraction were pooled and applied to PBE-94 (Pharmacia) and Heparin Sepharose (GE Healthcare) columns in series. PBE/Heparin flow through was dialyzed against Buffer B (HEPES-NaOH pH 7.8, 100 mM NaCl, 1 mM DTT, 0.1 mM EDTA, and 10% glycerol, containing 500 μM PMSF, 1 μg/mL Pepstatin, and 1 μg/mL Leupeptin). The protein was then loaded onto a 1 ml Heparin-Sepharose column (GE Healthcare) pre-equilibrated with Buffer B and eluted with a linear gradient of NaCl (100 mM to 1 M). Peak fractions containing hMutSγ were pooled and dialyzed against Buffer C (25 mM HEPES-NaOH pH 7.8, 100 mM NaCl, 1 mM DTT, 0.1 mM EDTA, 20% glycerol) and concentrated with 50 kDa cut-off Amicon centrifugal filters (Millipore). Aliquots were frozen in liquid nitrogen and stored at −80°C. Protein concentation was determined as described above.

Purification of hEXO1-D173A

hEXO1 (D173A) was prepared as described previously[16,31]. Sf9 insect cells were infected with baculovirus expressing hEXO1-D173A at 1×10^6 per mL and incubated at 27°C for 58 hrs. Cells were centrifuged at 2000 rpm for 10 minutes at 4°C, frozen in liquid nitrogen and stored at −80°C. All subsequent steps were carried out at <4°C. Cells were thawed on ice-cold water for 5 min and then resuspended in 5 volumes of lysis buffer A (20 mM KPO_4 pH 7.5, 150 mM KCL, 0.1 mM EDTA) with Protease inhibitors (500 uM PMSF, 1 ug/mL Pepstatin, 10 ug/mL Leupeptin, 10 ug/mL Aprotinin, 1ug/ml E-64). The cells were lysed using a dounce homogenizer for 5 strokes followed by gentle mixing on ice and addition of 50 % glycerol to a final concertation 10%, and 2 M KCl for a final concentration 150 mM.

The suspension was then incubated for an additional 15 min with gentle stirring. The extract was then clarified by centrifuged at 55,000 rpm for 30 min and loaded onto a 15-ml Q-Sepharose column (GE Healthcare), preequilibrated with Q-Sepharose buffer (20 mM KPO_4, pH 7.5, 100 mM KCl, 0.1 mM EDTA, 10% glycerol containing the same protease inhibitors used in the lysis buffer). The column was washed with 10 column volumes of Q-Sepharose buffer and eluted with a 5-column gradient of KCI gradient (100–400 mM) supplemented with 1mM DTT. hEXO1-D173A peak fractions were pooled and diluted two-fold with buffer B (20 mM KPO_4 pH 7.5, 150 mM KCL,10% glycerol 0.1 mM EDTA,1 mM DTT 0.5 mM PMSF, 1 ug/mL Pepstatin, 1ug/mL Leupeptin, 1 ug/mL Aprotinin) and fractionated on a 5 ml Heparin column (GE Healthcare) pre-equilibrated with buffer B. The column was washed with 20 column volumes of buffer B and eluted with a 10-column gradient of KCl (100–415 mM). Peak fraction were diluted to 150 mM KCl with buffer B and loaded onto a 1 ml MonoS column (GE Healthcare) pre-quilibrated with Mono S Buffer (20 mM KPO_4, pH 7.5, 150 mM KCL, 0.1 mM EDTA 10% glycerol, 0.5 mM PMSF, 1mM DTT, 1 ug/mL Pepstatin, 1 ug/mL Leupeptin, 1 ug/mL Aprotinin). Non-specifically bound protein was removed with Mono S Buffer and elution was performed with a 2-column volume linear KCl gradient (100–500 mM). hEXO1-D173A eluted at ~300 mM KCl on both the Heparin and MonoS columns. Peak fractions were subjected to Gel filtration chromatography on a S200 column (GE Healthcare) using S200 Buffer (20 mM KPO_4, pH 7.5, 300 mM KCL, 0.1 mM EDTA, 5% Glycerol, 0.5 mM PMSF and 1 ug/mL Leupeptin). Peak fractions were collected, supplemented with 20% glycerol and 1 mM DTT, flash-frozen in liquid nitrogen, and stored at −80 °C.

hPCNA and hRFC and hRPA

Purified hPCNA, hRFC and hRPA were generous gifts of Paul Modrich (Duke University), Jerry Hurwitz (MSKCC), and Steve Kowalczykowski (UC Davis), respectively.

DNA substrates

All oligonucleotides were obtained from Integrated DNA Technologies. Sequences are listed in Table 1. Oligonucleotides were 5’ end-labeled with [γ−32P] ATP (PerkinElmer Life Sciences) using T4 polynucleotide kinase (New England Biolabs). Unincorporated nucleotide was removed using G-50 Micro Columns (GE Healthcare). Substrate DNAs were annealed by combining end-labeled oligonucleotide with a 2-fold molar excess of the unlabeled complementary oligos. The end-labeled DNA substrates were then gel purified. Negatively supercoiled pUC19 and pUC-AT[32] plasmids (New England Biolabs) were prepared using standard protocols.

Nicking endonuclease assays

Endonuclease nicking assays were performed using 100 ng negatively supercoiled pUC19 or cruciform-containing pUC-AT plasmid DNA in 20 μl reaction mixtures containing 25 mM HEPES-NaOH pH 7.4, 50 mM NaCl, 1mM DTT, 5% glycerol, 0.2 mg/mL bovine serum albumin (NEB), indicated concentrations of purified proteins, and 5 mM metal cofactors ($MnCl_2$, $MgCl_2$, $ZnCl_2$, $CaCl_2$, $NiCl_2$, or $CoCl_2$, SIGMA). Where indicated, 0.5 mM ATP, ADP, AMP-PNP or ATP-γ-S (Sigma) was added. In this assay, a single nick is not distinguished from two or more nicks such that enzyme cleavage efficiency will be

underestimated when nicking levels are high. Also, plasmid relaxation by the first nick may make subsequent incisions less likely. Concerted nicking within a single enzyme ensemble would further complicate interpretation of nicking efficiencies. Thus, trends in nicking efficiency and patterns of stimulation are more important than absolute cleavage efficiencies, which should be interpreted with caution.

Reactions employing RFC-PCNA contained 25 mM HEPES-NaOH pH 7.4, 25 mM NaCl, 1mM DTT, 0.2 mg/mL bovine serum albumin BSA, 2% glycerol and 5 mM Mg^{2+} or Mn^{2+}. 25 nM hRFC, hPCNA, hEXO1-D173A, hMutLγ and hMutSγ and 0.5 mM ATP were added as indicated. Reactions were assembled on ice, incubated at 37˚C for indicated times, and stopped and deproteinized by adding 4 μl Stop buffer (200 mM EDTA and 2 mg/ml proteinase K, 2% SDS) and incubating for 20 min at 55˚C). Plasmid isoforms were separated by electrophoresis in 1% agarose gel on 1% TAE (1.25 V/cm ~ 2 hrs) and gels were stained with 0.5 μg/ml ethidium bromide. Gel images were acquired with a Fluro Chem 8900 (Alpha Innotech) and quantified using Image J.

EMSA DNA binding assay

Indicated concentrations of hMutLγ and 1 nM of ^{32}P-labeled DNA substrate were incubated in a 10 μl reaction mixture containing 25 mM HEPES (pH 7.8), 100 mM NaCl, 5 mM $MgCl_2$, 5% glycerol, 0.1 mg/ml BSA, 2 ng/μl poly(dI/dC) (SIGMA) and 1 mM DTT supplemented with indicated concentrations of nucleotides and/or divalent metal ions. Reaction mixtures were assembled on ice and incubated at 4°C for 10 min. To assemble hRPA coated ssDNA substrates, 1 nM of ^{32}P-labeled DNA substrates were combined in the reaction buffer described above together with indicated concentrations of hRPA and pre-incubated for 10 min at 4°C before adding hMutLγ and incubating for an additional 10 min. Bound and free DNA species were resolved by electrophoresis using non-denaturing 5% polyacrylamide gels in TAE buffer. Gels were dried on DE81 paper (Whatman) exposed to storage phosphor-storage screens and imaged using a Typhoon FLA 9000 imager (GE Healthcare). Fractions of mobility-shifted substrate were quantified, plotted and analyzed using Image J and GraphPad Prism software. The apparent equilibrium binding constants were obtained by fitting the data to the 1:1 binding equation:

$$Y = \frac{\left(K_D + [DNA] + [MLH] - \sqrt{(K_D + [DNA] + [MLH])^2 - 4 * [DNA]^*[MLH]}\right.}{2^*[DNA]}$$

- where K_D is the equilibrium dissociation constant, [DNA] is the concentration of DNA substrate (1 nM) and [MLH] is concentration of hMutLγ.

Denaturing urea PAGE analysis of HJ endonuclease reactions

Nuclease assays with 1 nM labeled HJ or nHJ substrates were performed in 15 μl volumes in presence of 5 mM Mg^{2+} and/or Mn^{2+}, 0.5 mM ATP, and 25 nM each protein in nuclease reaction buffer (above) for 30 min at 37°C. Reactions were stopped by the addition of EDTA (50 mM) and Proteinase K treatment was performed for 15 min at 55°C. 15 μl formamide dye (98% formamide, 10 mM EDTA, 0.1% bromophenol blue and 0.1% and xylene cyanol)

was added and reactions were denatured at 95°C for 5 min. The denatured products were separated on 15% denaturing polyacrylamide gel (National diagnostic lab Urea PAGE system) in 1X TBE buffer. The gels were rinsed twice in a solution containing 40% methanol, 10% acetic acid, and 5% glycerol, and then fixed in the same solution for 30 min at room temperature. Gels were then vacuum dried on 3 mm Chr Whatman paper, exposed to storage phosphor screen and scanned using a Typhoon Phosphor imager (FLA 9000, GE Healthcare).

Analysis of hMutLγ–hPCNA interaction

0.6 μg anti-PCNA antibody (Santa Cruz Biotechnology F2, 25280) was incubated with 20 μl Protein A beads and equilibrated in PBS buffer at 4°C for 2 hr with gentle mixing. The beads were washed twice with 100 μl PBS, mixed with 1 μg recombinant hPCNA and 0.5 μg hMutLγ in 100 μl binding buffer (20 mM HEPES pH7.4, 50 mM NaCl, 5% glycerol, 0.1 mM EDTA, 1 mM DTT), and incubated overnight at 4°C with gentle mixing. Supernatant was collected as unbound protein following a gentle spin at 1000 rpm for 2 min. Beads were washed three times with binding buffer (20 mM HEPES 7.4, 50 mM NaCl, 5% Glycerol, 0.1 mM EDTA, 1 mM DTT). The bound protein complexes were eluted in Laemmli buffer for 3 min at 95°C and separated on a 10% SDS-PAGE gel. The gel was rinsed with water, stained with SYPRO-Ruby (Lonza-50562) according to manufacturers recommendations, and imaged using a Typhoon FLA 9000 imager (GE Healthcare).

Mice

Mice were congenic with the C57BL/6J background and maintained and used for experiments according to the guidelines of Institutional Animal Care and Use Committees of the University of California Davis.

Mouse cytology

Surface-spread chromosomes of mouse spermatocytes were prepared from 18 days postpartum male mice using the drying-down technique as previously described[33]. Immuno-staining was performed as previously described[33] using the following primary and secondary antibodies: goat anti-SYCP3 (Santa Cruz Biotechnology, sc-20845; 1:200), rabbit anti-MSH4 (a gift from Dr. Paula Cohen; 1:200), mouse monoclonal anti-MLH1 (4C9C7) (Cell Signaling Technology, 3515S; 1:30), AMCA anti-goat (Jackson ImmunoResearch, 705–155-147; 1:50), Cy3 anti-rabbit (Jackson ImmunoResearch, 711–165-152; 1:100), and AlexaFluor647 anti-mouse (Jackson ImmunoResearch, 715–605-151; 1:100).

Image acquisition and analysis of mouse cytology

Chromosome spreads were imaged using a Zeiss Axioplan II microscope equipped with a 63 x Plan-Apochromat 1.4 NA objective, EXFO X-Cite metal halide light source, and a Hamamatsu ORCA-ER CCD camera. Images were processed and analyzed using Volocity software (Perkin Elmer). Focus counts and colocalization were determined manually. Early, mid and late pachytene stages were defined using standard criteria.

Yeast strains

Full genotypes of the *Saccharomyces cerevisiae* strains (SK1 background) used in this study are listed in Supplementary Table 2. Adaptation of the Auxin-Induced Degron (AID) system for use during meiosis has been described previously[34,35]. Fusion of a minimal *AID* cassette to *RFC1* was constructed using plasmid pHyg-AID*−9Myc as a template for PCR-mediated allele replacement, as previously described[35,36]. The estrogen-inducible *IN-NDT80 GAL4-ER* system has been described[35,37–39].

Meiotic time courses and DNA physical assays

Detailed protocols for meiotic time courses and DNA physical assays at the *HIS4::LEU2* locus have been described[40,41]. Degradation of Rfc1-AID was performed as pachytene cells were released from *IN-NDT80* arrest as described previously[35], with the following modifications: at 6.5 hours after induction of meiosis, $CuSO_4$ (100 mM stock in dH_2O) was added for a final concentration of 50 μM to induce expression of P_{CUP1}-*OsTIR1*, encoding the Tir1 E3 ligase. Then at 7 hours, auxin (3-indoleacetic acid, Sigma 13750, 2 M stock in DMSO) was added to one subculture at a final concentration of 2 mM to induce degradation of Rfc1-AID; and estradiol (5 mM stock, Sigma E2758 in ethanol) was added at a final concentration of 1 μM to both subcultures to induce *IN-NDT80*. At 7.5 hours, auxin was added again at 1 mM. Cell samples were collected to assay protein depletion, meiotic divisions, and recombination intermediates as described previously[35].

Western analysis

Whole cell extracts were prepared using the TCA extraction method, essentially as described[35]. Samples were analyzed by standard SDS-PAGE and Western blotting. Anti-c-myc monoclonal antibody (Roche; 11667149001) was diluted 1:1,000 to detect Rfc1-AID; Arp7 polyclonal antibody (Santa Cruz, SC-8961) was used at 1:5,000 dilution as a loading control. Secondary antibodies, used at 1:5,000 dilution, were IRDye® 800CW Donkey anti-Mouse IgG (LI-COR, 925–32212) and IRDye® 680LT Donkey anti-Goat IgG (LI-COR, 925–68024). Membranes were imaged with an Odyssey Infrared Imager (LI-COR). Quantification of protein bands was performed using Image Studio Lite 5.0.21 software.

Yeast cytology and chromosome spreading

Meiotic cells were collected at indicated time points and fixation and chromosome spread was performed essentially as described using 4% paraformaldehyde[42]. Immunostaining was performed as described[42]. Primary antibodies were anti-PCNA (Abcam; ab70472, 1:100), anti-Zip3 antibody (a gift from Dr. Akira Shinohara, 1:400) and anti-Zip1 (a gift from Dr. Scott Keeney, 1:400); all incubated overnight at room temperature in 100 ul TBS/BSA buffer (10 mM Tris PH7.5, 150 mM NaCl, 1% BSA) Secondary antibodies were anti-rabbit 568 (A11036 Molecular Probes, 1:1000), anti-mouse 488 (A11029 Molecular Probes, 1:1000), anti-rabbit 647 (A21245 Invitrogen), and anti-guinea pig 555 (A21435 Life Technologies); all for 1 hr at 37˚C. Coverslips were mounted with Prolong Gold antifade reagent (Invitrogen, P36930). Digital images were captured using a Zeiss Airyscan LSM800 with Axiocam and analyzed using Zen (blue edition); or a Zeiss Axioplan II microscope, Hamamatsu ORCA-ER CCD camera and analyzed using Volocity software. Co-localization

of protein foci was assigned to overlapping foci. Random colocalization (levels of colocalization by chance) were estimated by rotating the PCNA and Zip3 channels by 90° relative to one another and requantifying focus colocalization. Scatterplots were generated using the GraphPad program in Prism.

Statistics and Reproducibility

Images in Fig. 1c and Extended Data Figs. 5a are representative of the 28 nuclei analysed in Fig 1d. The images in Fig. 4b and 4d and Extended Data Fig. 10b are representative of the 7 independent time courses analysed in Fig. 4 e, f. The images in Fig. 4g are representative of the 25 analysed nuclei; similar staining patterns were seen for two independent experiments. Images in Extended Data Figs. 1b, and 4a are representative of at least 6 independent purifications of hMutLγ and hMutSγ, respectively. The image in Extended Data Fig. 4e reflects a single purification of hEXO1-D173A; results are comparable to those of Modrich and colleagues[16,31]. Images in Extended Data Fig. 6a and 6b analyse enzymes provided by collaborators and described in the accompanying references[43,44]. The image in Extended Data Fig. 6f is representative of three similar independent experiments. Images in Extended Data Fig. 8a and 8b are representative of two independent experiments as well as others using slightly different conditions.

Extended Data

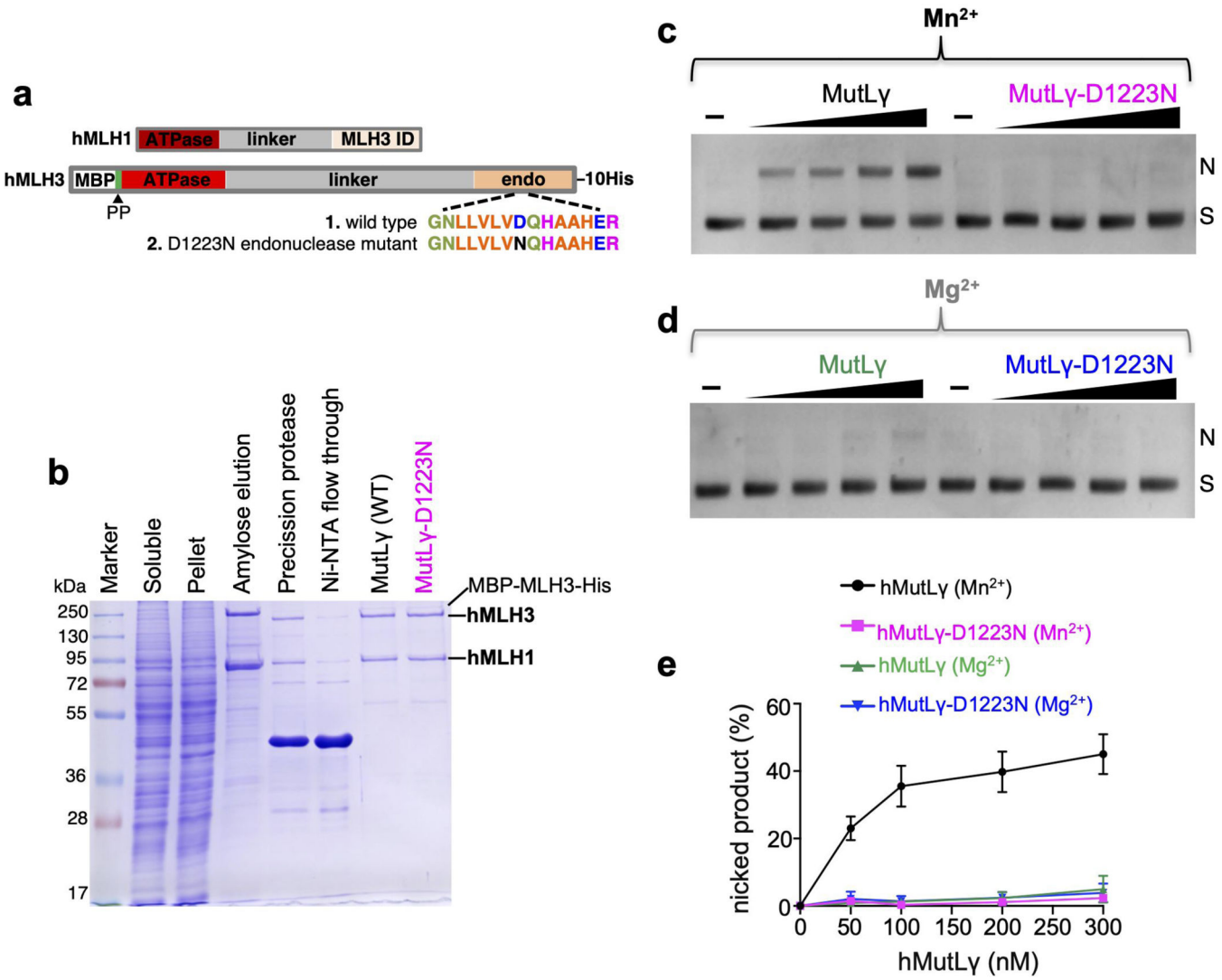

Extended Data Figure 1. Human MutLγ purification and endonuclease activity.

a, hMLH1 and hMLH3 expression constructs highlighting domain structure and affinity-purification tags: MLH3 ID, hMLH3 interaction domain; endo, endonuclease domain; MBP, maltose binding protein; PP, PreScission protease cleavage site; 10His, deca-histidine tag. Sequences of the conserved metal binding site for (1) wild-type and (2) the nuclease-dead D1223N mutant of MLH3 are also shown. **b,** Representative MutLγ purification steps monitored by 10% SDS-PAGE stained with Coomassie blue. Amylose enriched fractions were treated with Precission Protease, to cleave the maltose-binding protein tag, and then subjected to Ni-NTA affinity purification. **c, d,** Endonuclease assays for varying concentrations of hMutLγ and hMutLγ-D1223N (0–300 nM protein with (**c**) 5 mM Mn^{2+} or (**d**) Mg^{2+}) incubated at 37°C for 60 min. **e,** Quantitation of experiments represented in panels **c** and **d**. Means ± SEM are shown for three experiments after subtracting background nicked product from no-protein controls.

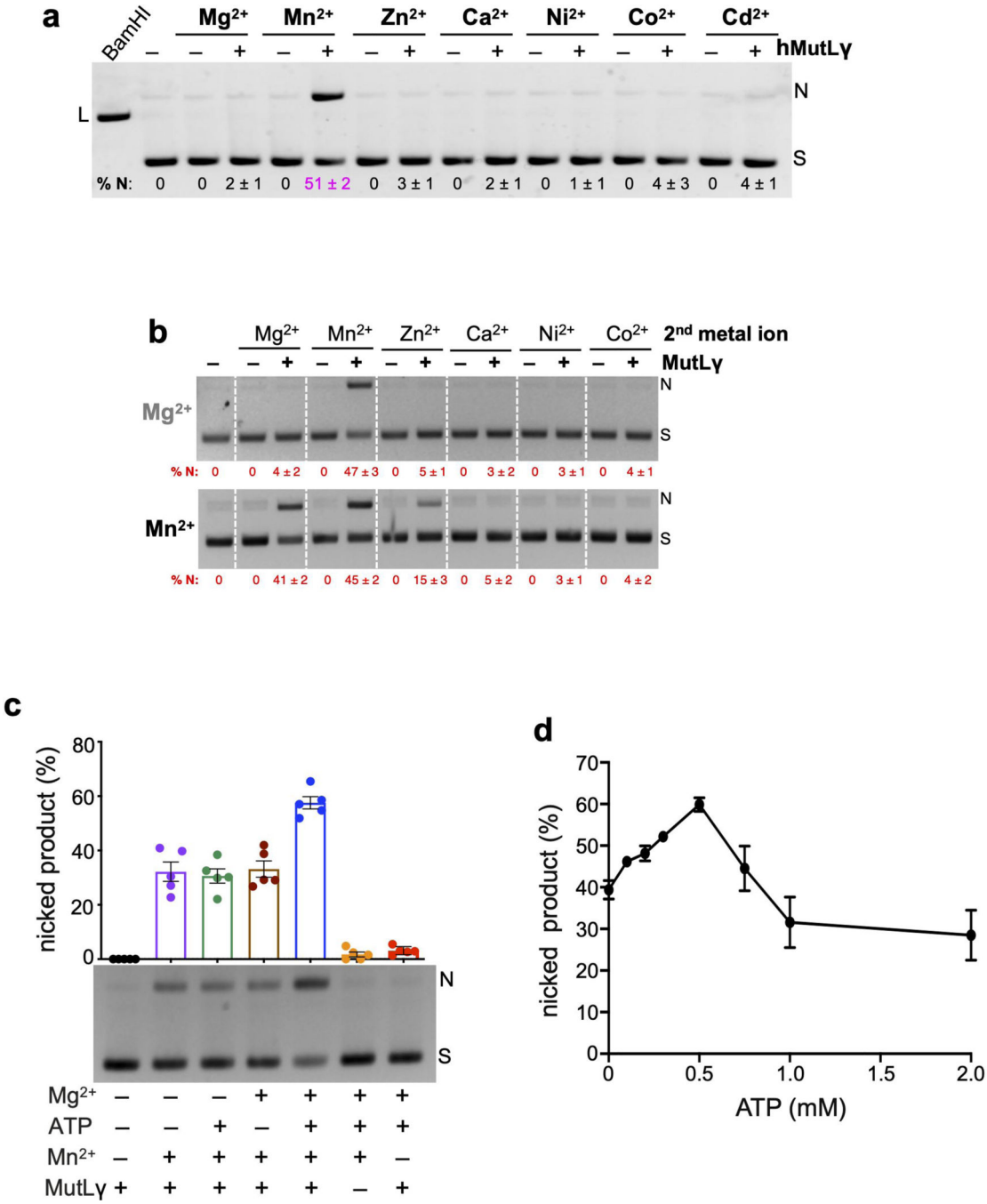

Extended Data Figure 2. MutLγ endonuclease activity with various metal cofactors and stimulation by ATP.

a, Representative gel image showing hMutLγ endonuclease assays with various metal ions (100 nM hMutLγ and 5 mM indicated divalent metal ions, incubated at 37°C for 90 min). Migration positions of supercoiled (S) plasmid and nicked (N) product are shown. For reference, plasmid linearized (L) with BamHI is also shown. % N, percent nicked product. Means ± SEM are shown for three experiments after subtracting background nicked product from no-protein controls. **b,** Representative endonuclease assays with 100 nM hMutLγ in 5

mM Mg^{2+} or Mn^{2+} with the addition of various second metal cofactors (5 mM). Reactions were incubated at 37°C for 90 min. Metals other than Mg^{2+} compete with Mn^{2+} to inhibit hMutL**γ** endonuclease activity. % N, percent nicked product. Means ± SEM are shown for three experiments. **c,** Representative gel image and quantification of hMutL**γ** endonuclease activity with and without ATP and metal cofactors (100 nM hMutL**γ**, 0.5 mM ATP and 5 mM Mn^{2+} and/or Mg^{2+} incubated at 37°C for 60 min). Means ± SEM are shown for five experiments. **d,** hMutL**γ** endonuclease activity with increasing ATP concentration. 100 nM hMutL**γ** was incubated with 5 mM Mn^{2+} and Mg^{2+} and indicated concentrations of ATP at 37°C for 60 min. Endonuclease stimulation was optimal with 0.5 mM ATP, while higher concentrations were inhibitory. Means ± SEM are shown for three independent experiments.

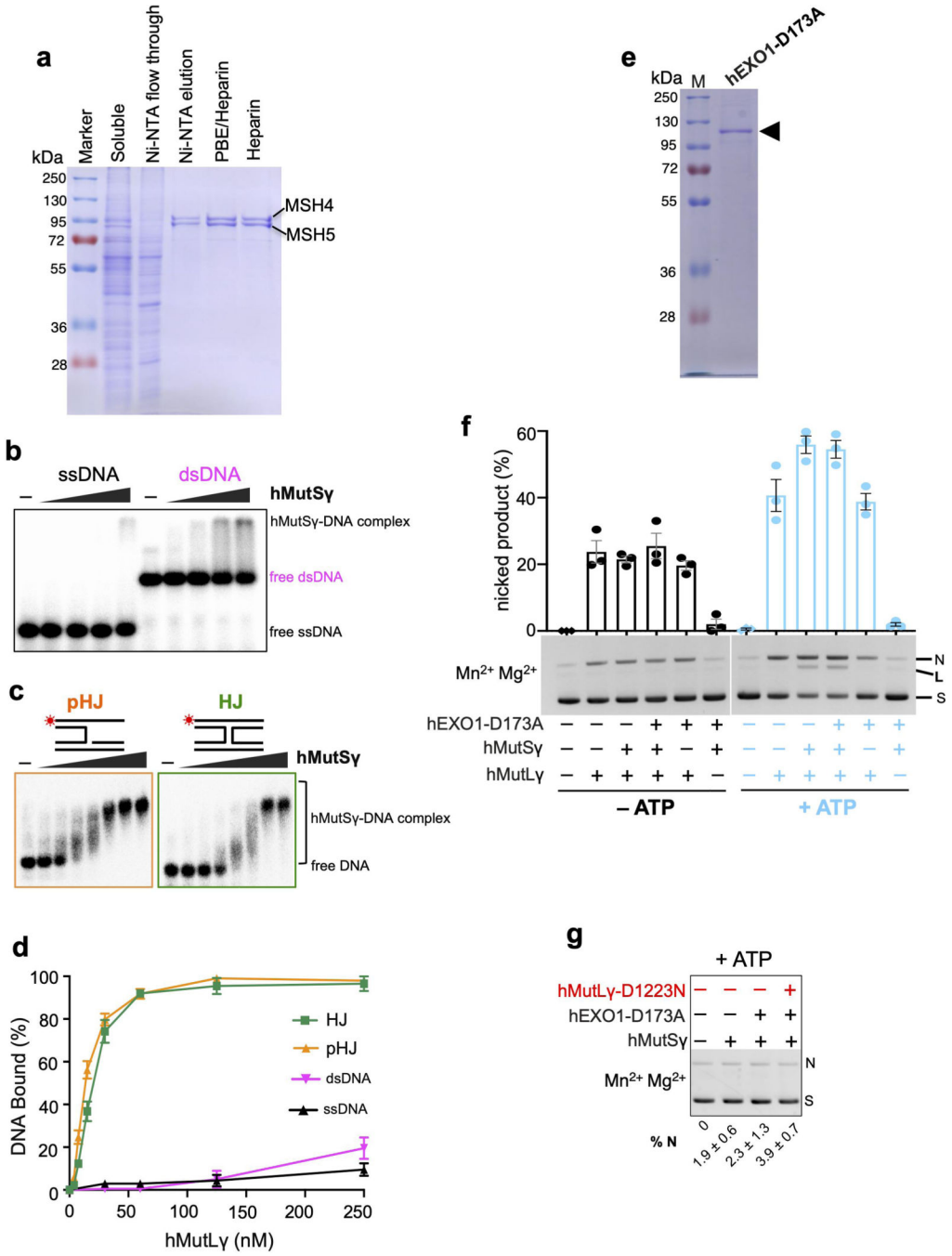

Extended Data Figure 3. Purification and characterization of human MutSγ.

a, Representative hMutSγ purification steps monitored by 10% SDS-PAGE stained with Coomassie blue. **b,** Representative images of electrophoretic mobility shift assays (EMSAs) analyzing hMutSγ binding to 80mer single and double-stranded DNAs. Binding reactions contained 1 nM ^{32}P-labeled DNA, 100 mM NaCl and 5 mM Mg^{2+} and were incubated on ice for 10 min. Bound and free DNA species were resolved by non-denaturing 5% polyacrylamide gel electrophoresis and processed for imaging. **c,** Representative images of EMSAs analyzing hMutSγ binding to pro-HJ and Holliday junction structures. Terminally

^{32}P-labeled strands are indicated by asterisks. **d,** Quantification of the EMSAs represented in panels **b** and **c** showing means ± SEM for three independent experiments. **e,** SDS-PAGE analysis of purified nuclease-dead hEXO1-D173A (10% gel stained with Coomassie). **f,** Endonuclease assays with varying mixtures of hMutLγ, hMutSγ and hEXO1-D173A, with and without ATP (50 nM each protein, 0.5 mM ATP, 5 mM Mn^{2+} and Mg^{2+} incubated at 37°C for 60 min). Means ± SEM are shown for three experiments. **g,** Negative control endonuclease assays with nuclease-dead hMutLγ-D1223N, hMutSγ and hEXO1-D173A. Average percent nicking (%N) ± SEM are shown for three experiments.

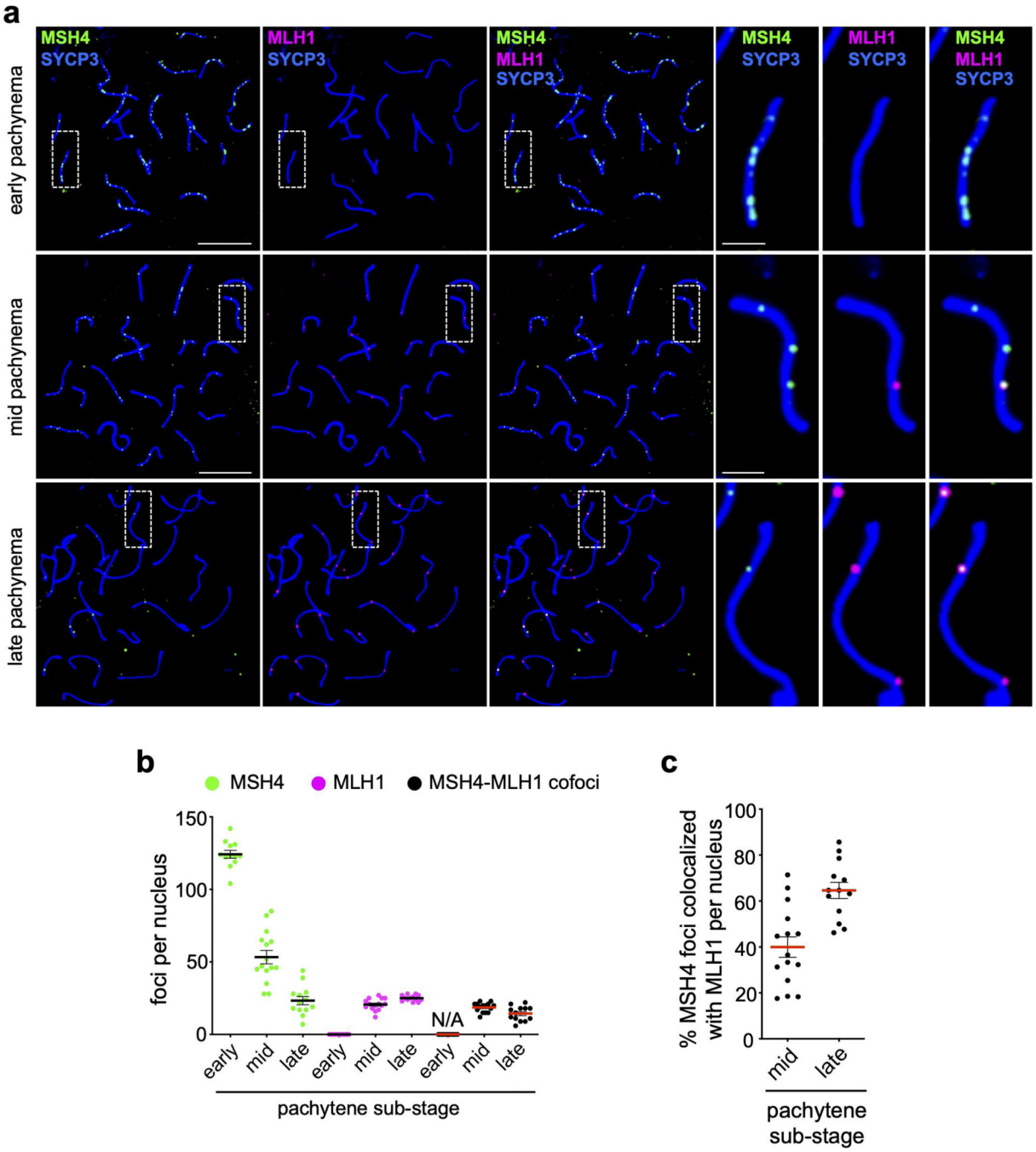

Extended Data Figure 4. Colocalization of MutLγ and MutSγ in mouse spermatocytes.

a, Representative images of surface-spread spermatocyte chromosomes from the indicated pachytene substages, immuno-stained for MSH4 (green), MLH1 (magenta) and the chromosome axis marker SYCP3 (blue). Magnified panels show individual pairs of synapsed chromosomes. Scale bars, 10 and 2 μm, respectively. Arrowheads indicate crossover-specific MLH1 foci that colocalize with MSH4. **b,** Quantification of MSH4 and MLH1 foci and MSH4-MLH1 cofoci in early, mid and late-pachytene stages (n=12, 15 and 13 nuclei, respectively; error bars indicate means ± SEM; N/A, not applicable because

MLH1 foci were not observed in early pachytene). **c,** Percent of MSH4 foci that are colocalized with MLH1 in mid and late pachytene nuclei (n=12, 15 and 13 nuclei, respectively; error bars indicate means ± SEM). The percentage of co-foci increases as the majority of MSH4 foci disappear in late pachynema.

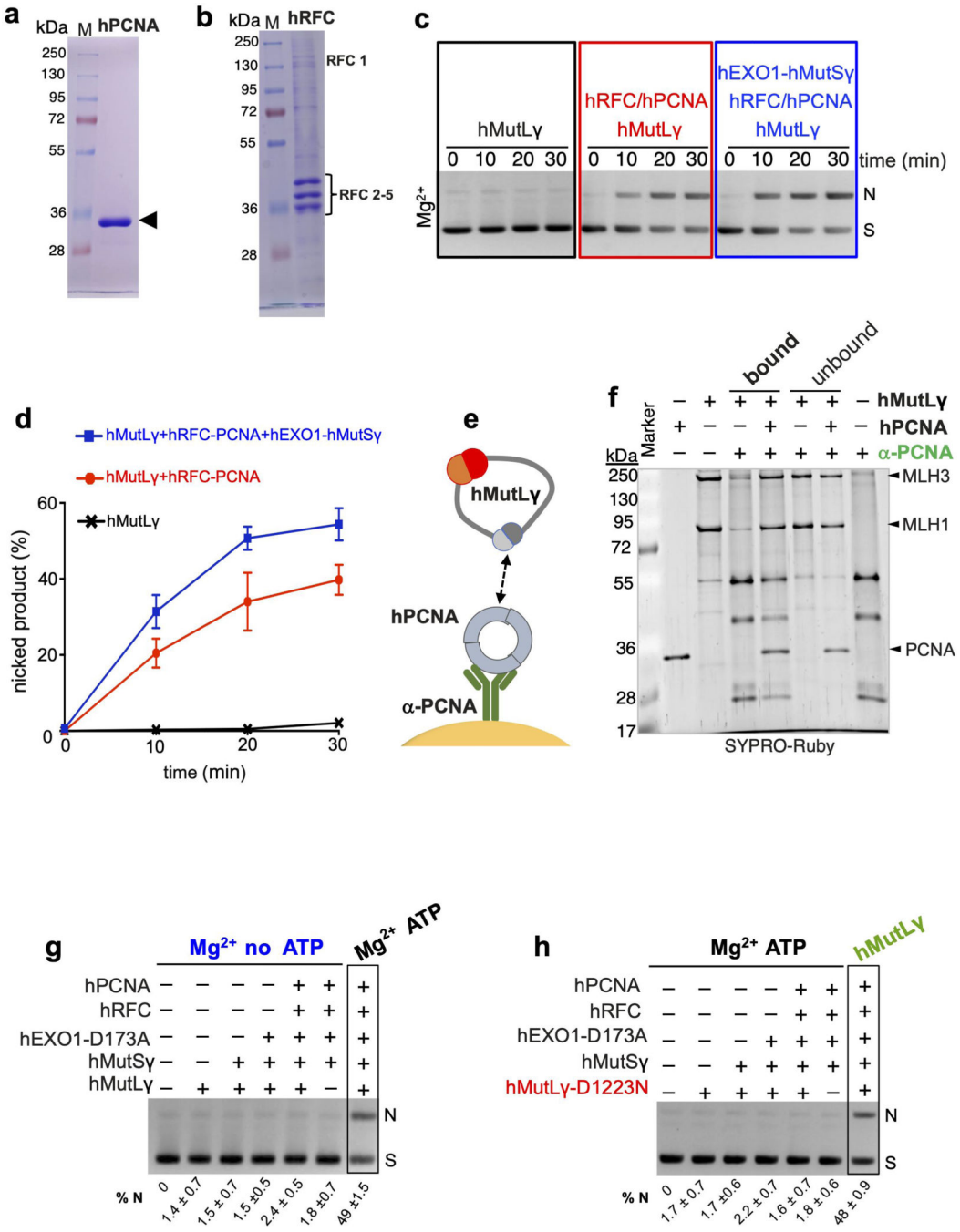

Extended Data Figure 5. RFC-PCNA activates the latent endonuclease activity of hMutLγ in Mg^{2+}.

a, b, SDS-PAGE analysis of purified hPCNA and hRFC (10% gels stained with Coomassie).

c, d, Time course analysis of hMutLγ endonuclease activity in Mg^{2+}, with and without

hRFC/PCNA and hMutSγ-EXO1-D173A. Representative gel images (**c**) and quantification of three independent experiments (**d**, means ± SEM) are shown. Reactions contained 25 nM indicated proteins, 0.5 mM ATP and 5 mM Mg^{2+} and were incubated at 37°C for the indicated times. **e,** Experimental scheme to analyze hMutLγ-hPCNA interaction in solution. **f,** SYPRO-Ruby stained SDS-PAGE analysis of hMutLγ-hPCNA interaction. **g,** ATP dependence of ensemble nicking reactions showing a representative gel image and quantification of % nicking (% N, means ± SEM from three independent experiments). Reaction conditions were as described for panels **c** and **d** but without ATP, except in the positive control reaction. **h,** Dependence of ensemble nicking reactions on the MLH3 endonuclease active site. Representative gel images for reactions with nuclease-dead hMutLγ-D1223N and quantification of % nicking (% N) are shown (means ± SEM from three independent experiments). Reactions contained 25 nM indicated proteins, 0.5 mM ATP and 5 mM Mn^{2+} and were incubated at 37°C for 30 min. A reaction containing wild-type hMutLγ was included as a positive control.

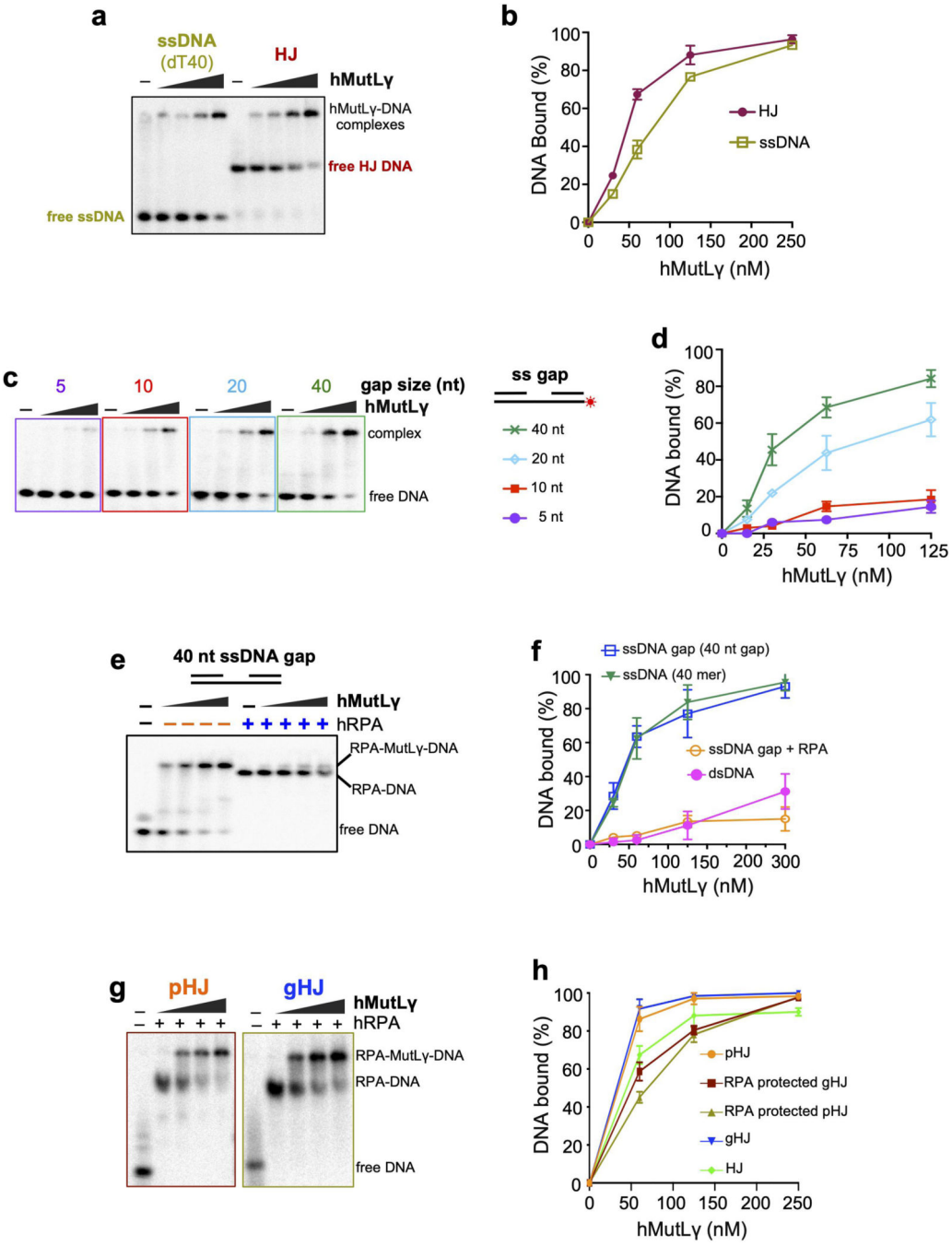

Extended Data Figure 6. hMutLγ binding to single-stranded DNA.

a, Representative image of EMSAs comparing hMutLγ binding to ssDNA and Holliday junctions. **b,** Quantification of the EMSAs represented in panel **a**. Means ± SEM for three independent experiments are shown. Binding reactions contained 1 nM ^{32}P-labeled DNA, 100 mM NaCl and 5 mM Mg^{2+} and were incubated on ice for 10 min. Bound and free DNA species were resolved by non-denaturing 5% polyacrylamide gel electrophoresis and processed for imaging. **c,** Representative images of EMSAs analyzing hMutLγ binding to 80mer DNAs containing single-strand gaps of varying size. To define the minimal single-

strand gap that is efficiently bound by hMutLγ, 80 nt linear DNAs containing gaps of varying lengths were tested. **d,** Quantification of the EMSAs represented in panel **c** showing means ± SEM for three independent experiments. Significant binding was not detected for gaps of 5 and 10 nt, but 20 and 40 nt gaps were bound efficiently. Notably, this minimal binding site is similar to that bound by the canonical ssDNA binding protein RPA. **e,** Representative images of EMSAs for hMutLγ binding to an 80mer DNA containing a 40 nucleotide gap, with or without prior incubation with RPA. **f,** Quantification of the EMSAs represented in panel **e** shows that hMutLγ binds a 40 nt gap with almost identical affinity as a 40mer single stranded DNA; and that pre-incubation with RPA blocks hMutLγ binding. Error bars show means ± SEM for three independent experiments. **g,** Representative images of EMSAs for hMutLγ binding to pro-HJs and gapped-HJs that were pre-incubated with RPA. To test whether the branched and ssDNA binding activities are autonomous, gHJ and pHJ substrates were pre-incubated with RPA and then used as binding substrates for hMutLγ. RPA-gHJ and RPA-pHJ complexes were still readily bound by hMutLγ. **h,** Quantification of the EMSAs represented in panel **g** and in main figure Fig. 3a shows that ssDNA and junction binding activities of hMutLγ are largely independent. Error bars show means ± SEM for three independent experiments.

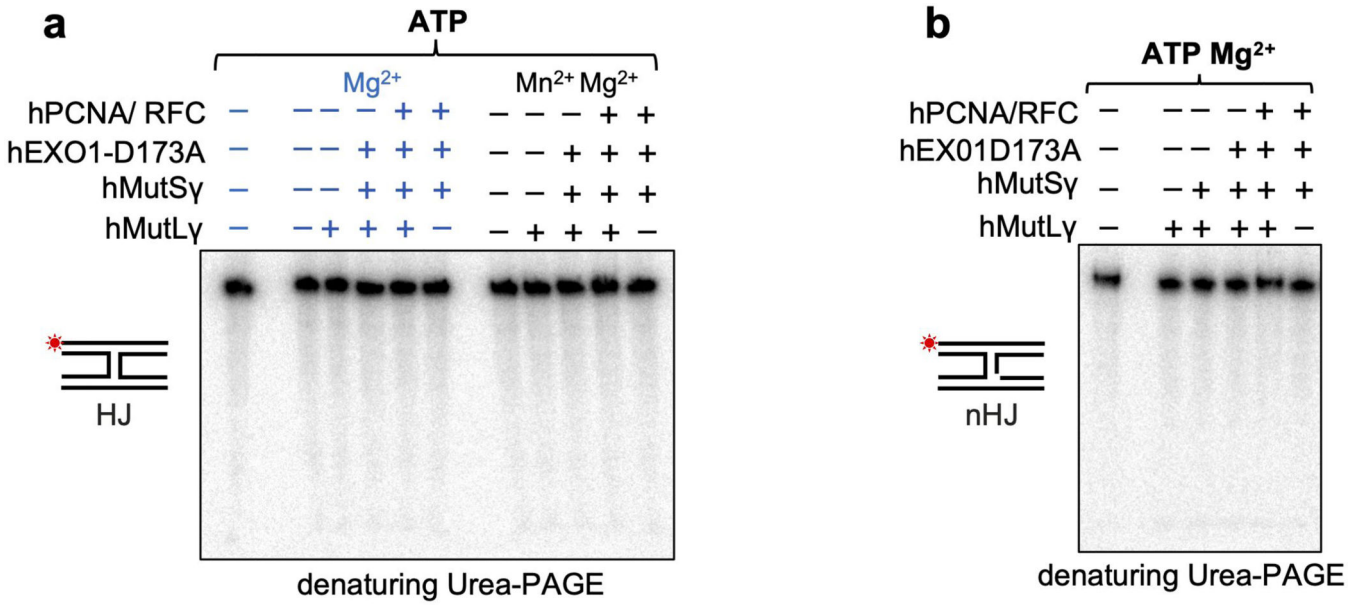

Extended Data Figure 7. Model Holliday junctions are not incised by hMutLγ.

a and **b,** Representative gel images of ensemble endonuclease reactions with HJ and nicked HJ substrates. Reactions contained 25 nM indicated proteins, 0.5 mM ATP and 5 mM Mg^{2+}/Mn^{2+}, and were incubated at 37°C for 30 min. The reaction products were analyzed on a 15% denaturing polyacrylamide gel to detect strand nicking at any position. Nicking was not detected consistent with non-denaturing gels showing that model HJ and nHJ structures are not resolved by the hMutLγ ensemble (not shown).

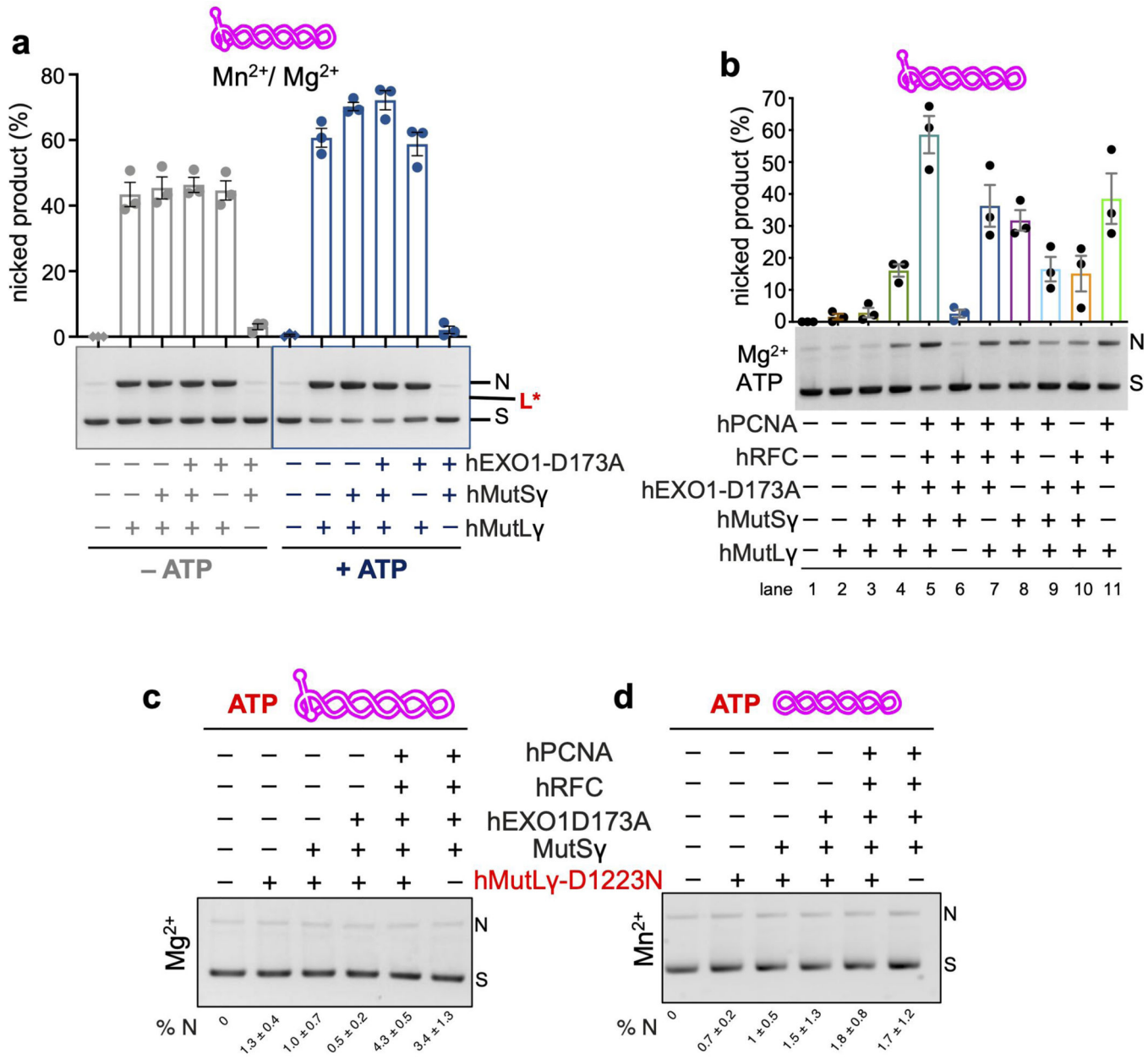

Extended Data Figure 8. Cleavage of supercoiled plasmid containing a cruciform structure.

a, Endonuclease assays with pUC(AT) and varying mixtures of hMutLγ, hMutSγ and hEXO1-D173A, with and without ATP (50 nM each protein, 0.5 mM ATP, 5 mM Mn^{2+} and 5 mM Mg^{2+}, incubated at 37°C for 60 min). Means ± SEM are shown for three experiments. Under these conditions, pUC(AT) is incised 1.3–1.7-fold more efficiently than the corresponding reactions with pUC19 (also see Fig. 3e). Notably, the linear cleavage product seen with the pUC19 substrate (expected position indicated by L*; see Fig. 1e) was not observed. We suggest that this reflects a more physiological nicking reaction because MutSγ and MutLγ can interact with the cruciform structure. Thus, both the efficiency of nicking and the nature of the incision products are altered when a Holliday junction is present. **b,** The interdependent nature of stimulation by MutSγ and hEXO1-D173A. Representative gel

image and quantification of ensemble endonuclease reactions with using pUC(AT) as substrate and Mg^{2+} as the sole metal cofactor. Reactions contained 25 nM indicated proteins, 0.5 mM ATP and 5 mM Mg^{2+} and were incubated at 37°C for 30 min. Means ± SEM are shown for three experiments. **c** and **d,** Negative control ensemble endonuclease assays for pUC(AT) (**b**) and pUC19 (**c**) containing nuclease-dead hMutLγ-D1223N. Reactions contained 25 nM indicated proteins, 0.5 mM ATP and 5 mM Mg^{2+} or Mn^{2+} and were incubated at 37°C for 30 min. Average percent nicking (%N) ± SEM is shown for three independent assays.

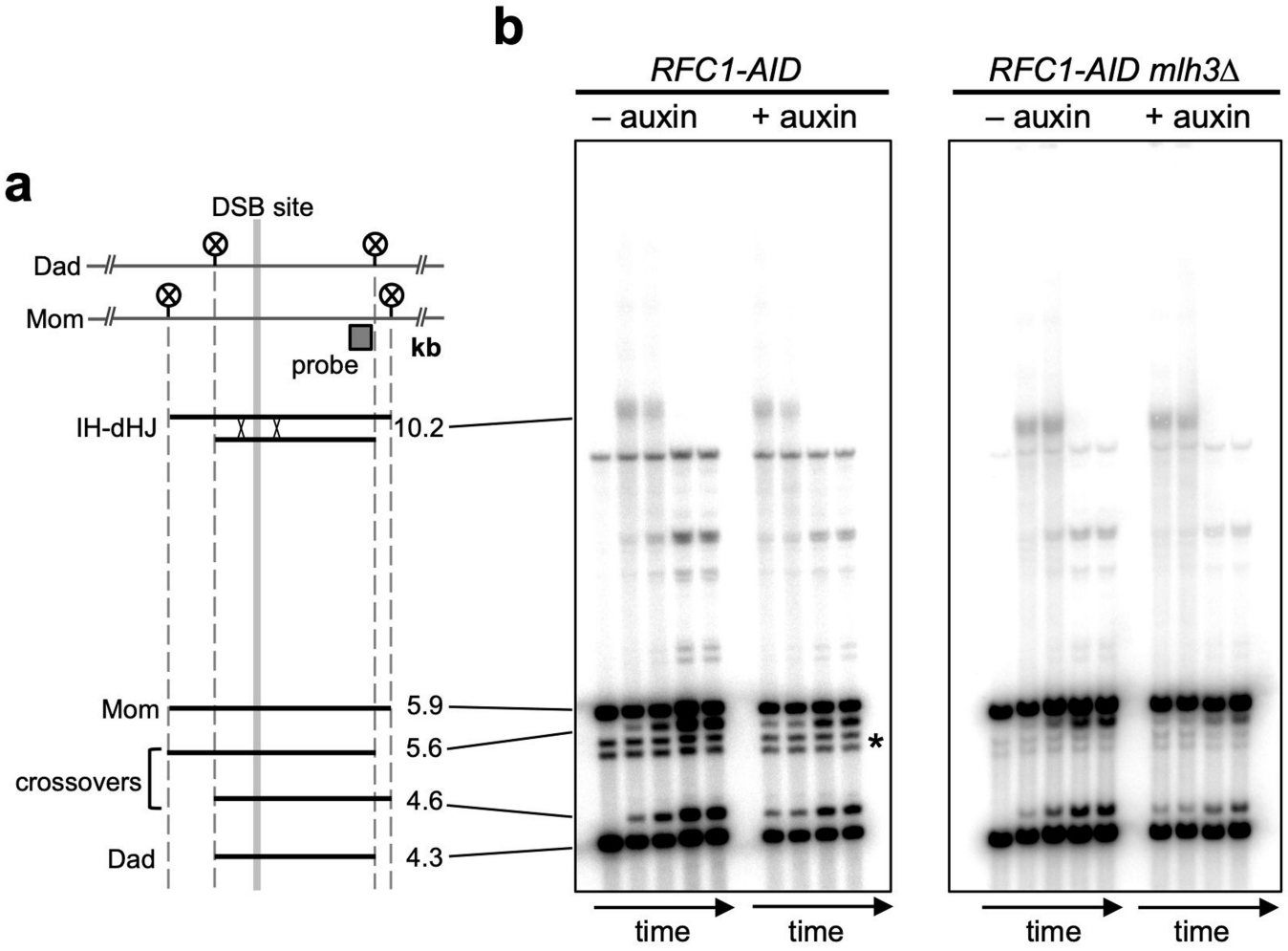

Extended Data Figure 9. Physical assay system for analysis of meiotic recombination in budding yeast.

a, Map of the *HIS4:LEU2* recombination hotspot locus highlighting the initiating DSB site, *Xho*I restriction sites (circled Xs) and the position of the probe used in Southern blotting. Sizes of diagnostic fragments are shown to the right. **b,** Representative 1D gel Southern blot images for analysis of crossovers and dHJs in *RFC1-AID* and *RFC1-AID mlh3Δ* strains, with and without the addition of auxin to trigger Rfc1-AID degradation. Time points are 0, 7, 8, 9, and 11 hours after induction of meiosis.

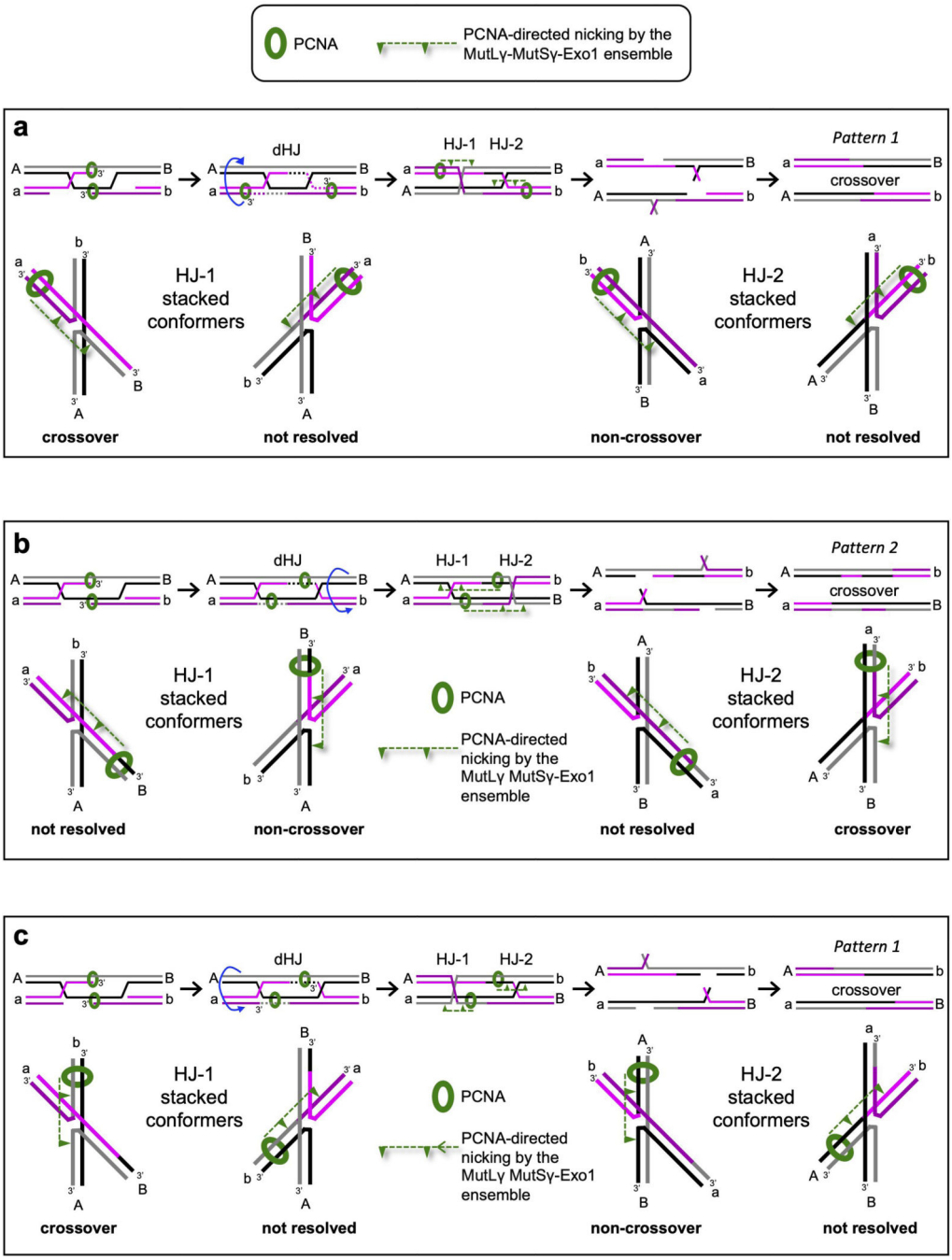

Extended Data Figure 10. Model variants.

Comparison of variations on the basic theme that MutLγ mediates crossover-specific dHJ resolution by catalyzing strand-specific incisions on both sides of the two HJs. **a,** The model presented in Fig. 4h is shown for comparison. This version has recombination-associated DNA synthesis tracts terminating outside the dHJ. PCNA at these termini direct the MutLγ-MutSγ-Exo1 ensemble to incise upstream (5') specifically on the strands with DNA synthesis, maintaining this specificity across the stacked junctions (lower panels). Resolution of HJ-1 results in a crossover while HJ-2 is resolved as a non-crossover.

Importantly, this version of the model produces only “Pattern 1” crossovers, shown by Llorente and colleagues to be promoted by MutLγ [3]. **b,** On the other hand, a more canonical scheme, with synthesis tracts and associated PCNA molecules located within the dHJ produces “Pattern 2” crossovers, thereby disfavoring this version of the model. **c,** Pattern 1 crossovers are also produced by a variant of the model in which MutLγ-MutSγ-Exo1 incises downstream (3’) of the internal synthesis tracts. However, this polarity is opposite to that established for MMR[12,13].

Supplementary Material

Refer to Web version on PubMed Central for supplementary material.

Acknowledgements

We thank Paul Modrich (Duke), Jerry Hurwitz (MSKCC), Ken Marians (MSKCC), Steve Kowalczykowski (UCD) Paula Cohen (Cornell), Scott Keeney (MSKCC) and Akira Shinohara (Osaka University) for reagents; Petr Cejka (Università della Svizzera italiana) for reagents and communicating unpublished data; Bertrand Llorente and members of the Hunter Lab for support and discussions. This work was supported by NIH NIGMS grant GM074223 to N.H. S.O. was supported by NIH NIGMS T32 Training Program in Molecular and Cellular Biology 5T32GM007377 and an F31 Ruth L. Kirschstein National Research Service Award 1F31GM125106. M.I. was supported by a Japan Society for the Promotion of Science postdoctoral fellowship for research abroad. N.H. is an Investigator of the Howard Hughes Medical Institute.

REFERENCES

1. Hunter N. Meiotic Recombination: The Essence of Heredity. Cold Spring Harbor perspectives in biology 7, a016618 (2015). [PubMed: 26511629]
2. Allers T. & Lichten M. Differential timing and control of noncrossover and crossover recombination during meiosis. Cell 106, 47–57 (2001). [PubMed: 11461701]
3. Marsolier-Kergoat MC, Khan MM, Schott J, Zhu X. & Llorente B. Mechanistic view and genetic control of DNA recombination during meiosis. Molecular cell 70, 9–20 (2018). [PubMed: 29625041]
4. Szostak JW, Orr-Weaver TL, Rothstein RJ & Stahl FW The double-strand-break repair model for recombination. Cell 33, 25–35 (1983). [PubMed: 6380756]
5. Nishant KT, Plys AJ & Alani E. A mutation in the putative MLH3 endonuclease domain confers a defect in both mismatch repair and meiosis in *Saccharomyces cerevisiae*. Genetics 179, 747–755 (2008). [PubMed: 18505871]
6. Zakharyevich K, Tang S, Ma Y. & Hunter N. Delineation of joint molecule resolution pathways in meiosis identifies a crossover-specific resolvase. Cell 149, 334–347 (2012). [PubMed: 22500800]
7. Toledo M. et al. A mutation in the endonuclease domain of mouse MLH3 reveals novel roles for MutLgamma during crossover formation in meiotic prophase I. PLoS genetics 15, e1008177 (2019). [PubMed: 31170160]
8. Ranjha L, Anand R. & Cejka P. The Saccharomyces cerevisiae Mlh1-Mlh3 heterodimer is an endonuclease that preferentially binds to Holliday junctions. The Journal of biological chemistry 289, 5674–5686 (2014). [PubMed: 24443562]
9. Rogacheva MV et al. Mlh1-Mlh3, a meiotic crossover and DNA mismatch repair factor, is a Msh2-Msh3-stimulated endonuclease. The Journal of biological chemistry 289, 5664–5673 (2014). [PubMed: 24403070]
10. Manhart CM et al. The mismatch repair and meiotic recombination endonuclease Mlh1-Mlh3 is activated by polymer formation and can cleave DNA substrates in trans. PLoS biology 15, e2001164 (2017). [PubMed: 28453523]

11. Snowden T, Acharya S, Butz C, Berardini M. & Fishel R. hMSH4-hMSH5 recognizes Holliday Junctions and forms a meiosis-specific sliding clamp that embraces homologous chromosomes. Molecular cell 15, 437–451 (2004). [PubMed: 15304223]
12. Iyer RR, Pluciennik A, Burdett V. & Modrich PL DNA mismatch repair: functions and mechanisms. Chem Rev 106, 302–323 (2006). [PubMed: 16464007]
13. Kolodner RD A personal historical view of DNA mismatch repair with an emphasis on eukaryotic DNA mismatch repair. DNA repair 38, 3–13 (2016). [PubMed: 26698650]
14. Manhart CM & Alani E. Roles for mismatch repair family proteins in promoting meiotic crossing over. DNA repair 38, 84–93 (2016). [PubMed: 26686657]
15. Kadyrova LY & Kadyrov FA Endonuclease activities of MutLalpha and its homologs in DNA mismatch repair. DNA repair 38, 42–49 (2016). [PubMed: 26719141]
16. Kadyrov FA, Dzantiev L, Constantin N. & Modrich P. Endonucleolytic function of MutLalpha in human mismatch repair. Cell 126, 297–308 (2006). [PubMed: 16873062]
17. Pluciennik A. et al. PCNA function in the activation and strand direction of MutLalpha endonuclease in mismatch repair. Proceedings of the National Academy of Sciences of the United States of America 107, 16066–16071 (2010). [PubMed: 20713735]
18. Pillon MC et al. Structure of the endonuclease domain of MutL: unlicensed to cut. Molecular cell 39, 145–15 (2010). [PubMed: 20603082]
19. Pillon MC et al. The sliding clamp tethers the endonuclease domain of MutL to DNA. Nucleic acids research 43, 10746–10759 (2015). [PubMed: 26384423]
20. Claeys Bouuaert C. & Keeney S. Distinct DNA-binding surfaces in the ATPase and linker domains of MutLgamma determine its substrate specificities and exert separable functions in meiotic recombination and mismatch repair. PLoS genetics 13, e1006722 (2017). [PubMed: 28505149]
21. Kadyrova LY, Gujar V, Burdett V, Modrich PL & Kadyrov FA Human MutLgamma, the MLH1-MLH3 heterodimer, is an endonuclease that promotes DNA expansion. Proceedings of the National Academy of Sciences of the United States of America 117, 3535–3542 (2020). [PubMed: 32015124]
22. Kadyrov FA et al. Saccharomyces cerevisiae MutLalpha is a mismatch repair endonuclease. The Journal of biological chemistry 282, 37181–37190 (2007). [PubMed: 17951253]
23. Sonntag Brown M, Lim E, Chen C, Nishant KT & Alani E. Genetic analysis of mlh3 mutations reveals interactions between crossover promoting factors during meiosis in baker's yeast. G3 3, 9–22 (2013). [PubMed: 23316435]
24. Lahiri S, Li Y, Hingorani MM & Mukerji I. MutSgamma-Induced DNA Conformational Changes Provide Insights into Its Role in Meiotic Recombination. Biophys J 115, 2087–2101 (2018). [PubMed: 30467025]
25. Gray S. & Cohen PE Control of Meiotic Crossovers: From Double-Strand Break Formation to Designation. Annual review of genetics 50, 175–210 (2016).
26. Zakharyevich K. et al. Temporally and biochemically distinct activities of Exo1 during meiosis: double-strand break resection and resolution of double Holliday junctions. Molecular cell 40, 1001–1015 (2010). [PubMed: 21172664]
27. Schaetzlein S. et al. Mammalian Exo1 encodes both structural and catalytic functions that play distinct roles in essential biological processes. Proceedings of the National Academy of Sciences of the United States of America 110, E2470–2479 (2013). [PubMed: 23754438]
28. Mukherjee S, Wright WD, Ehmsen KT & Heyer WD The Mus81-Mms4 structure-selective endonuclease requires nicked DNA junctions to undergo conformational changes and bend its DNA substrates for cleavage. Nucleic acids research 42, 6511–6522 (2014). [PubMed: 24744239]
29. Sisakova A, Altmannova V, Sebesta M. & Krejci L. Role of PCNA and RFC in promoting Mus81-complex activity. BMC Biol 15, 90 (2017). [PubMed: 28969641]
30. Zhang L. et al. Topoisomerase II mediates meiotic crossover interference. Nature 511, 551–556 (2014). [PubMed: 25043020]
31. Genschel J, Bazemore LR & Modrich P. Human exonuclease I is required for 5' and 3' mismatch repair. The Journal of biological chemistry 277, 13302–13311 (2002). [PubMed: 11809771]
32. Eichman BF, Vargason JM, Mooers BH & Ho PS The Holliday junction in an inverted repeat DNA sequence: sequence effects on the structure of four-way junctions. Proceedings of the National

Academy of Sciences of the United States of America 97, 3971–3976 (2000). [PubMed: 10760268]

33. Kolas NK et al. Localization of MMR proteins on meiotic chromosomes in mice indicates distinct functions during prophase I. The Journal of cell biology 171, 447–458 (2005). [PubMed: 16260499]
34. Nishimura K, Fukagawa T, Takisawa H, Kakimoto T. & Kanemaki M. An auxin-based degron system for the rapid depletion of proteins in nonplant cells. Nature methods 6, 917–922 (2009). [PubMed: 19915560]
35. Tang S, Wu MKY, Zhang R. & Hunter N. Pervasive and essential roles of the Top3-Rmi1 decatenase orchestrate recombination and facilitate chromosome segregation in meiosis. Molecular cell 57, 607–621 (2015). [PubMed: 25699709]
36. Morawska M. & Ulrich HD An expanded tool kit for the auxin-inducible degron system in budding yeast. Yeast 30, 341–351 (2013). [PubMed: 23836714]
37. Benjamin KR, Zhang C, Shokat KM & Herskowitz I. Control of landmark events in meiosis by the CDK Cdc28 and the meiosis-specific kinase Ime2. Genes & development 17, 1524–1539 (2003). [PubMed: 12783856]
38. Carlile TM & Amon A. Meiosis I is established through division-specific translational control of a cyclin. Cell 133, 280–291 (2008). [PubMed: 18423199]
39. Louvion JF, Havaux-Copf B. & Picard D. Fusion of GAL4-VP16 to a steroid-binding domain provides a tool for gratuitous induction of galactose-responsive genes in yeast. Gene 131, 129–134 (1993). [PubMed: 8370533]
40. Owens S, Tang S. & Hunter N. Monitoring Recombination During Meiosis in Budding Yeast. Methods Enzymol 601, 275–307 (2018). [PubMed: 29523236]
41. Hunter N. & Kleckner N. The single-end invasion: an asymmetric intermediate at the double-strand break to double-holliday junction transition of meiotic recombination. Cell 106, 59–70 (2001). [PubMed: 11461702]
42. Grubb J, Brown MS & Bishop DK Surface Spreading and Immunostaining of Yeast Chromosomes. J Vis Exp, e53081 (2015). [PubMed: 26325523]
43. Dzantiev L. et al. A defined human system that supports bidirectional mismatch-provoked excision. Molecular cell 15, 31–41 (2004). [PubMed: 15225546]
44. Cai J. et al. Reconstitution of human replication factor C from its five subunits in baculovirus-infected insect cells. Proceedings of the National Academy of Sciences of the United States of America 93, 12896–12901 (1996). [PubMed: 8917516]

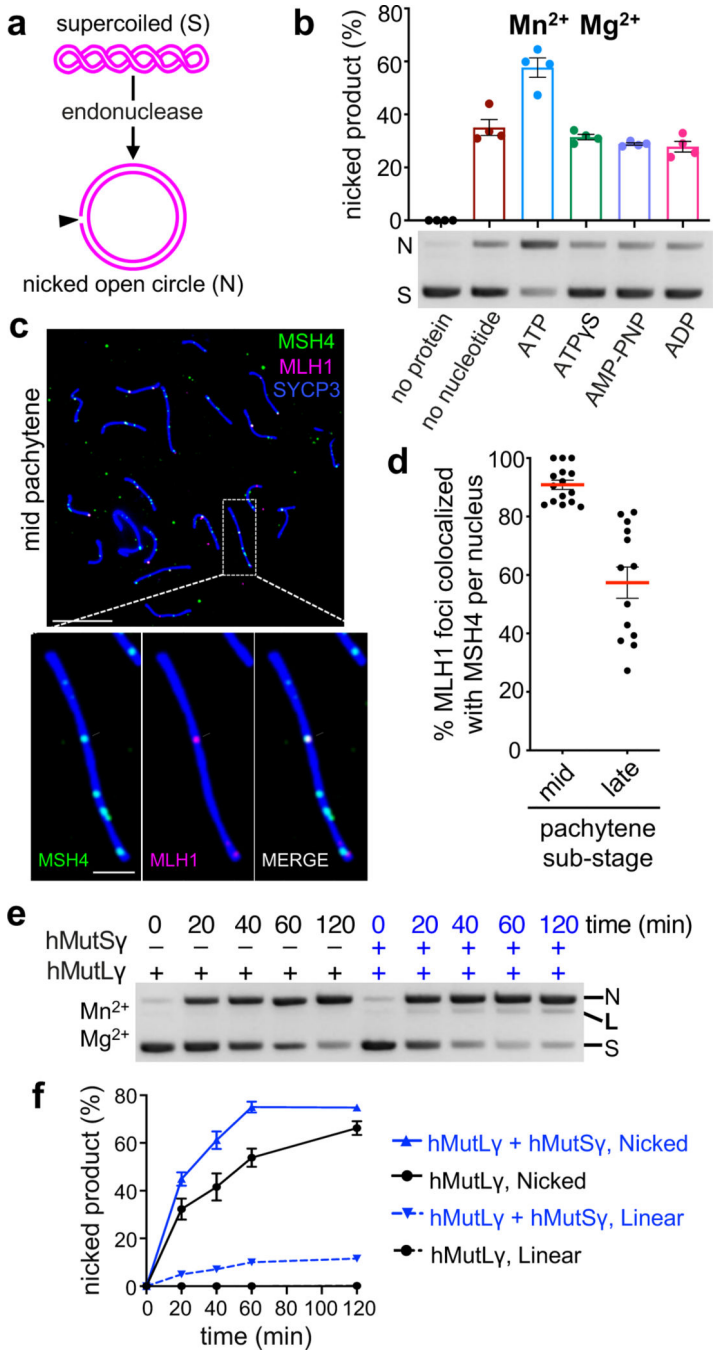

Figure 1. hMutLγ endonuclease is stimulated by ATP hydrolysis and hMutSγ.

a, Supercoiled plasmid nicking assay. **b,** Representative gel image and quantification of hMutLγ endonuclease activity with indicated nucleotides and analogs (100 nM hMutLγ, 0.5 mM nucleotide/analog, 5 mM Mn^{2+} and 5 mM Mg^{2+} incubated at 37°C for 60 min). Migration positions of supercoiled (S) plasmid and nicked (N) product are indicated. Quantification shows means ± SEM for four experiments. **c,** Representative image of surface-spread chromosomes from a mid-pachytene stage mouse spermatocyte, immuno-stained for MSH4 (green), MLH1 (magenta) and chromosome axis marker SYCP3 (blue).

Magnified panels show an individual pair of synapsed chromosomes in which a single crossover-specific MLH1 focus is colocalized with a MSH4 focus. Scale bars: 10 and 2 μm respectively. **d,** Quantification of MLH1-MSH4 colocalization (means ± SEM) in mid- and late-pachytene stage nuclei (n=15 and 13 nuclei, respectively). **e,** Representative gel image of a time-course analysis of hMutL**γ** endonuclease activity, with and without hMutS**γ** (100 nM hMutL**γ** ± 100 nM hMutS**γ**, 0.5 mM ATP, 5 mM Mn^{2+} and Mg^{2+} incubated at 37°C for indicated times). The linearized plasmid product (L) is indicated. **f,** Quantification of five independent time-course experiments (means ± SEM).

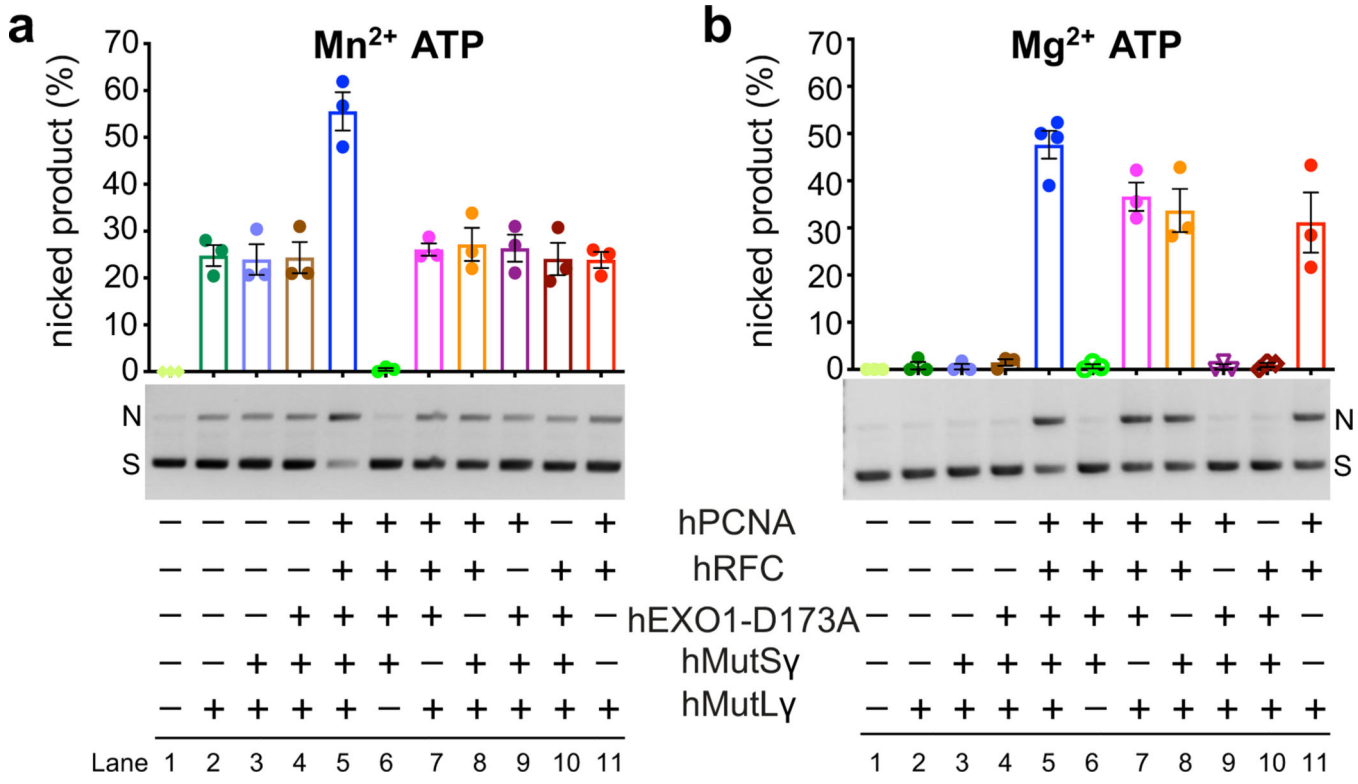

Figure 2. hRFC and hPCNA activate hMutLγ endonuclease activity.

a, Representative gel image and quantification of ensemble endonuclease reactions with Mn^{2+} as the sole metal cofactor. Reactions contained 25 nM indicated proteins, 0.5 mM ATP and 5 mM Mn^{2+} and were incubated at 37°C for 30 min. **b,** Representative gel image and quantification of reactions with Mg^{2+} as the sole metal cofactor. Reaction conditions were as described for panel **a**, but with 5 mM Mg^{2+} instead of Mn^{2+}. For **a** and **b**, means ± SEM are shown for three or four independent experiments.

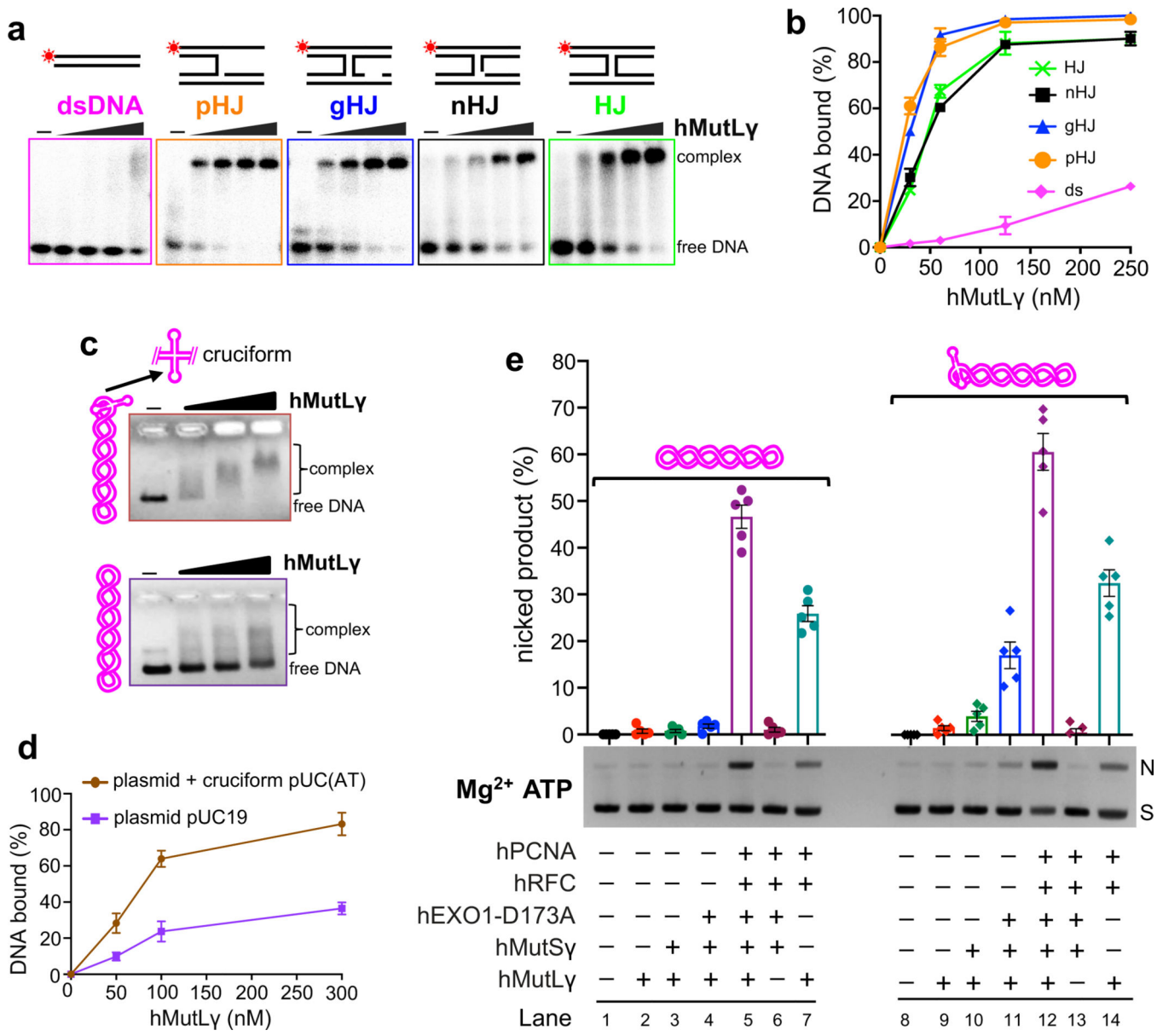

Figure 3. Holliday junctions are specifically bound by hMutLγ and modulate its endonuclease activity.

a, Representative images of electrophoretic mobility shift assays (EMSAs) analyzing hMutLγ binding to control double-stranded DNA and the illustrated branched structures. Terminally ^{32}P-labeled strands are indicated by asterisks. **b,** Quantification of the EMSAs represented in panel **a** showing means ± SEM for three independent experiments. **c,** Representative images of EMSAs for hMutLγ binding to pUC(AT) and pUC19 supercoiled plasmids. **d,** Quantification of the EMSAs represented in panel **c**. Error bars show means ± SEM for three independent experiments. **e,** Representative gel image and quantification of endonuclease reactions with pUC19 or pUC(AT), and Mg^{2+} as the sole metal cofactor. Reactions contained 25 nM indicated proteins, 0.5 mM ATP and 5 mM Mg^{2+} and were incubated at 37°C for 30 min. Means ± SEM are shown for five independent experiments.

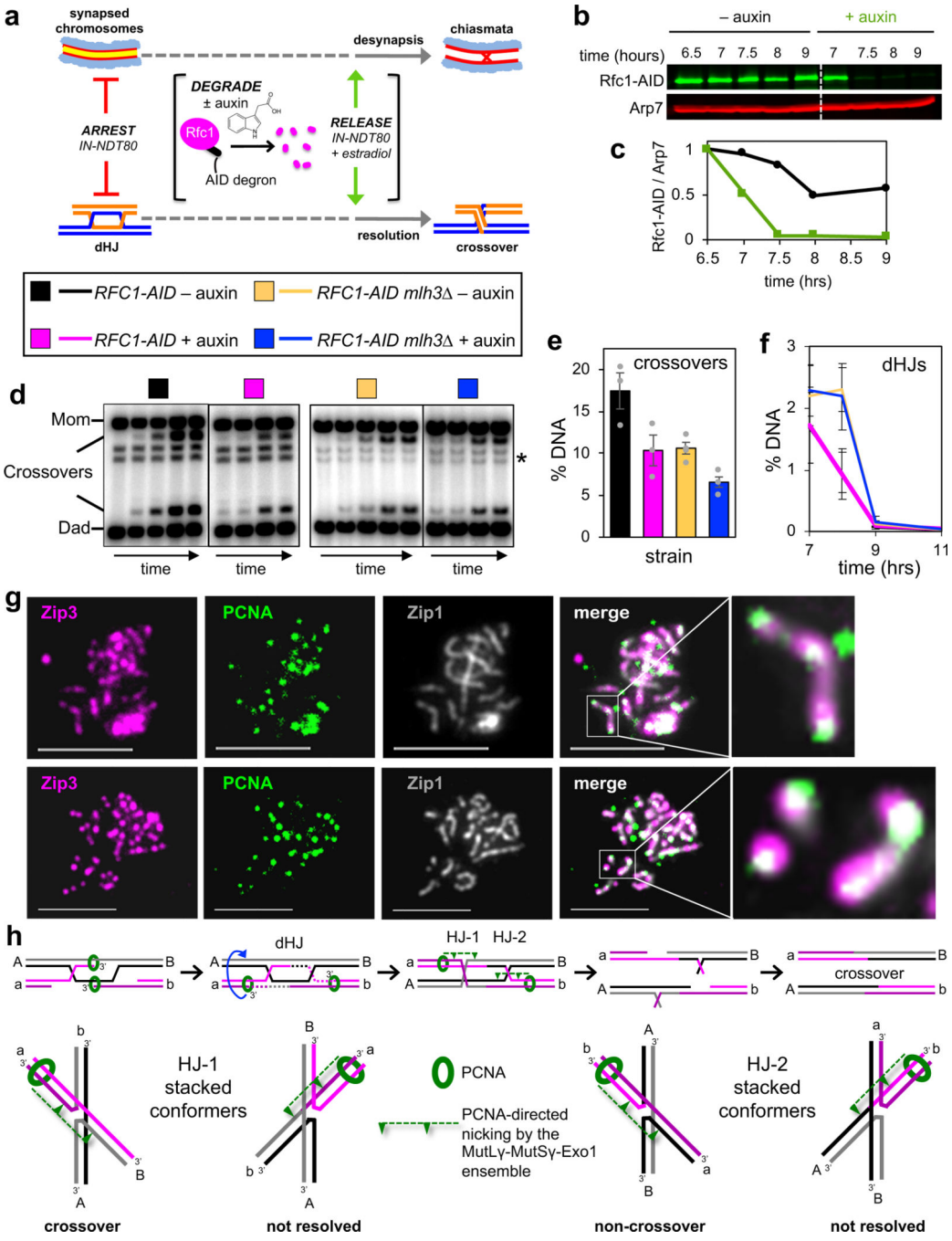

Figure 4. RFC-PCNA promotes crossing over *in vivo*.

a, Regimen to degrade Rfc1-AID during late meiotic prophase as dHJs are resolved. 6.5 hrs after induction of meiosis, copper was added to induce expression of the E3 ligase Tir1. At 7 hours, auxin was added to trigger degradation of Rfc1-AID; and estradiol was added to induce *IN-NDT80* and release cells from pachytene arrest. **b,** Representative Western analysis of Rfc1-AID in cells with and without addition of auxin. **c,** Quantification of the experiment shown in Figure 4b. **d,** Representative Southern blot images of crossover analysis at the *HIS4::LEU2* recombination hotspot. Time points are 0, 7, 8, 9, and 11 hours

after induction of meiosis. * background cross hybridizing bands. **e,f,** Quantification of crossover products and dHJ intermediates. “% DNA” is percentage of total hybridizing DNA signal, with error bars representing means ± SEM for three (*RFC1-AID* ± auxin) or four (*RFC1-AID mlh3Δ* ± auxin) experiments. **g,** Representative images of surface spread meiotic nuclei immunostained for PCNA (green), the crossover marker Zip3 (magenta), and synaptonemal complex protein Zip1 (grey). Scale bars = 5 μm. PCNA and Zip3 foci were quantified from 25 nuclei with pachytene morphologies (linear Zip1 staining). Magnified panels show individual synaptonemal complexes with colocalizing PCNA and Zip3 signals. **h,** Model of crossover-specific dHJ resolution during meiosis. Top row: PCNA molecules loaded during dHJ maturation direct MutLγ to catalyze strand-specific nicking on either side of the two HJs. This pattern of incisions, in combination with migration about the junction points, results in crossover-specific resolution. Bottom row: PCNA-directed MutLγ incisions resolve only one of the two stacked-X HJ conformers, which may be favored by factors such as MutSγ. Alternatively, conformers may freely interconvert. For HJ-1, resolution always produces a crossover; while for HJ-2, non-crossover products are always formed.